An Extended Finite Element Method for Modelling Dislocation Interactions with Inclusions

by

Pawan Veeresh

A Thesis Presented in Partial Fulfillment
of the Requirements for the Degree
Master of Science

Approved November 2016 by the
Graduate Supervisory Committee:

Jay Oswald, Chair
Hanqing Jiang
Yongming Liu

ARIZONA STATE UNIVERSITY

December 2016

ABSTRACT

A method for modelling the interactions of dislocations with inclusions has been developed to analyse toughening mechanisms in alloys. This method is different from the superposition method in that infinite domain solutions and image stress fields are not superimposed. The method is based on the extended finite element method (XFEM) in which the dislocations are modelled according to the Volterra dislocation model. Interior discontinuities are introduced across dislocation glide planes using enrichment functions and the resulting boundary value problem is solved through the standard finite element variational approach. The level set method is used to describe the geometry of the dislocation glide planes without any explicit treatment of the interface geometry which provides a convenient and an appealing means for describing the dislocation. A method for estimating the Peach-Koehler force by the domain form of J-integral is considered. The convergence and accuracy of the method are studied for an edge dislocation interacting with a free surface where analytical solutions are available. The force converges to the exact solution at an optimal rate for linear finite elements. The applicability of the method to dislocation interactions with inclusions is illustrated with a system of Aluminium matrix containing Al_2Cu precipitates. The effect of size, shape and orientation of the inclusions on an edge dislocation for a difference in stiffness and coefficient of thermal expansion of the inclusions and matrix is considered. The force on the dislocation due to a hard inclusion increased by 8% in approaching the sharp corners of a square inclusion than a circular inclusion of equal area. The dislocation experienced 24% more force in moving towards the edges of a square shaped inclusion than towards its centre. When the areas of the inclusions were halved, 30% less force was exerted on the dislocation. This method was used to analyse interfaces with mismatch strains. Introducing eigenstrains equal to 0.004 to the elastic mismatch increased the force by 15 times for a circular inclusion. The

energy needed to move an edge dislocation through a domain filled with circular inclusions is 4% more than that needed for a domain with square shaped inclusions.

ACKNOWLEDGMENTS

I would like to thank Dr. Jay Oswald for the opportunity and his constant support of this project. I am also appreciative of Dr. Ilaksh Adlakha, Dr. Vipin Agrawal, Dr. Xiao Liao, Dr. Rui Yuan, Benyamin Gholami and Yiyang Li for their timely help. I would like to extend my gratitude to my parents for their endless encouragement.

TABLE OF CONTENTS

LIST OF FIGURES

Figure Page

Figure Page

Figure Page

Figure Page

Chapter 1

INTRODUCTION

1.1 Introduction to Dislocations

In crystalline solids, atoms or molecules repeat themselves in fixed distances. The position of such atoms or molecules is governed by the cell parameters. But in reality, these atoms or molecules are not perfectly arranged. The periodic patterns are interrupted by crystallographic defects and these defects strongly influence many properties of a material. Elastic fields of one such defect were originally defined by Volterra in 1907; through the displacement of a cut cylinder, Volterra introduced several types of dislocations.

Point defects are generally related to a single lattice point. For example, vacancy defects are due to vacant lattice points which would be otherwise occupied in a perfect crystal and interstitial defects are caused by atoms that occupy sites where there usually are no atoms. Larger defects in ordered structures are called dislocations. Dislocations are line defects around which atoms of an ordered structure are skewed. Three scientists working independently, Taylor (1934), Orowan and Polanyi devised the term 'dislocation' to refer to a defect on an atomic scale in 1934.

The best description of a dislocation is obtained from a study of its formation in a crystalline lattice. A crystal plane is cut and one-half of it is slid across the other half by a lattice vector. The halves are then fit back together to form the new, distorted lattice. The lattice structure itself is almost perfect except near the plane of cut. The resulting line imperfection near the plane of cut is a dislocation line. Three types of dislocation lines may be formed. If the atoms over the cut surface are shifted in

a direction perpendicular to the plane of cut, an edge dislocation is created in the lattice; if the shift is parallel, a screw dislocation is created; if the shift is neither parallel nor perpendicular to the plane of cut, a mixed dislocation is created. Just by looking at the interior of the crystal, it is not possible to tell as to how the dislocation was created. The structure and properties of a dislocation, therefore, do not depend on how they were introduced in the crystal lattice.

Edge dislocations can also be created by adding an extra half plane of atoms in a crystal structure. This causes the adjacent plane of atoms to distort and bend themselves around the edge of the terminating plane so that the crystal structure is ordered everywhere else. The inter-atomic bonds are distorted only in the immediate vicinity of the dislocation. This is similar to inserting half a sheet of paper into a stack of papers. The defect is visible at the edge of the half sheet.

Screw dislocations are slightly harder to visualise. In the process of creating a screw dislocation, the atom planes perpendicular to the dislocation line are turned into a helical ramp. The screw dislocation itself is a pole about which the ramp circles. The atom planes are analogous to the floors of a parking structure. A car would have to travel on a spiral upward/downward slope to access other floors. The motion of a screw dislocation is also due to the application of shear stress. The defect line moves perpendicular to the direction of applied stress and atom displacement. The total deformation of both the edge and screw dislocation is the same.

A dislocation is described by the line direction, which is the direction along the top or bottom edge of the extra half plane, and the Burgers vector, which describes the magnitude and direction of distortion of the lattice. In an edge dislocation, the Burgers vector is perpendicular to the line direction, i.e., the defect line movement is parallel to the direction of applied stress and atom displacement. The line direction and Burgers vector of the dislocation in most materials in neither parallel nor

perpendicular. Such dislocations known as mixed dislocation, containing aspects of both edge and screw dislocations.

Dislocations allow deformation to occur at a much lower stress than in an ordered structure. Dislocation movement is, therefore, important in understanding non-linear bulk material behaviour and plasticity. A dislocation moves by a small amount at a time. The dislocation in the top or bottom half of the crystal moves by slipping one plane at a time to the left or right from its original position. In the course of slipping one plane at a time, the dislocation propagates across the crystal. This movement of the dislocation ultimately causes one-half of the crystal to move with respect to the other half. However, only a small portion of the bonds are broken at any given time resulting in smaller forces deforming the crystal instead of breaking all the bonds at once which would require a much larger force. There is an alternative mechanism of dislocation motion that allows an edge dislocation to move out of its slip plane and onto a plane directly above or below the slip plane. The driving force for a dislocation climb is the movement of vacancies in a lattice. If a vacancy is present next to the edge of a half plane of atoms in an edge dislocation, the atom in the plane closest to the vacancy will jump and fill the vacancy. This shift causes a vacancy in the line of half plane of atoms known as a positive climb due to vacancy annihilation. In contrast, a vacancy can also be absorbed in the edge of half plane of atoms known as a negative climb.

Dislocations are created as a result of breaking of atomic bonds along a line in a crystal lattice. This phenomenon requires the simultaneous breaking of multiple bonds which demands a concentrated stress. Irregularities at the grain boundary and uneven stress distribution at the crystal surface are more likely to produce dislocations.

The linear elastic theory accurately describes the long-range elastic stresses but it

breaks down in the immediate region surrounding the dislocation centre, known as the dislocation core. The dislocation core properties have been studied extensively due to their important role in crystal plasticity. The core properties influence dislocation movement which then affects the ductility or brittleness of solids. Two types of theoretical approaches have been employed to study dislocation core properties. The first method using direct atomistic models, though considerably more accurate, is computationally more expensive for studying dislocation properties. The second method is based on the Volterra model of dislocations which offers a better alternative.

Volterra Model of Dislocations

An edge dislocation is inserted by introducing a cut along the crystal plane ($y = 0$) such that the boundary of the cut is out of the plane (z-axis). Let $u^+(x)$ and $u^-(x)$ be the displacement fields on the upper and lower surfaces respectively. The dislocation is created by shifting the lower surface with respect to the upper surface by the Burgers vector and then reattaching the two surfaces together. The misfit across the plane would be defined to be equal to $u^+(x) - u^-(x)$. $u(x)$ is then a step function in the Volterra dislocation,

$$u^+(x) - u^-(x) = \begin{cases} -b, & \text{if } x < 0 \\ 0, & \text{otherwise} \end{cases} \tag{1.1}$$

The distribution of misfit across the plane of cut is described by the dislocation density, which for the Volterra dislocation is a delta function. This distribution although simple is inaccurate by being singular along the dislocation line itself. This prediction is non-physical and the Peierls-Nabarro model (P-N model) corrects the singularity by spreading the Burgers vector around the dislocation centre. The actual shape of the dislocation density distribution is now selected in the P-N model to

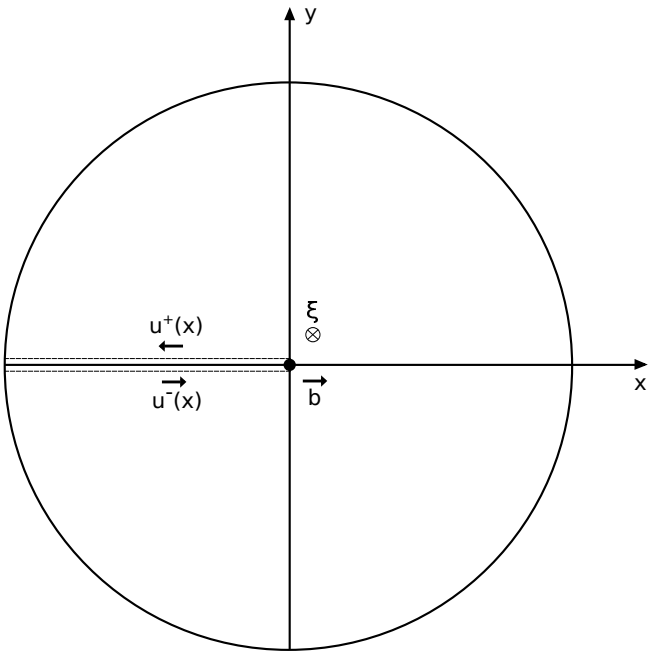

Figure 1.1: The Volterra edge dislocation introduced in a crystal. (from Bulatov and Cai (2006))

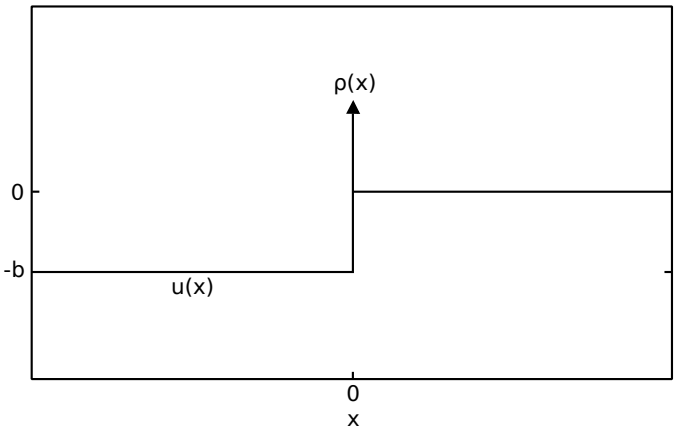

Figure 1.2: In the Volterra model of a dislocation, distribution of $u(x)$ across the cut plane is a step function and its distribution density $\rho(x) = \frac{\mathrm{d}u(x)}{\mathrm{d}x}$ is a delta function. (from Bulatov and Cai (2006))

consider the non-linearity involved in the dislocation core. The basic idea of the P-N model is to separate the dislocated solid into two elastic parts across their common interface known as the glide plane. The P-N model attempts to find the displacement field across the glide plane that would minimize the total energy of the solid. One of the considerable achievements of the P-N model is that it provides a reasonable estimate of the dislocation core size. Belytschko and Gracie (2007) considered compatible (P-N model) and incompatible (Volterra model) enrichments to model dislocations in systems with arbitrary material interfaces. The accuracy of the two enrichments was found to be of the same order for the problems considered, suggesting the details of the core representation did not affect the results significantly.

1.2 Review of the Extended Finite Element Method

In the analysis by conventional finite element method, the continuum is discretized into a series of nodes connected in a specific way, called the mesh. However, in the presence of internal defects like interfaces, voids, inclusions, etc., meshing becomes difficult. The element boundary must now coincide with the geometric edge of the defect which induces some distortion in the element. Also, defects like cracks can only propagate along an element edge and not along an arbitrary path.

Within the framework of the finite element method, a re-meshing technique was traditionally used for modelling cracks. Swenson and Ingraffea (1988) presented a finite element method that allowed discrete cracks to propagate through the mesh in arbitrary directions through re-meshing. This was an improvement over earlier methods that assumed cracks to propagate along pre-defined mesh lines (usually a straight line). This re-meshing technique was performed near the crack-tip to align the element edges with the crack faces and proved to be quite arduous in the case of dynamic crack propagation where a new mesh is generated each time the crack

grows. In addition, a dynamic solution depicts an evolving history requiring the need to preserve said history when the mesh is updated. This is achieved by mapping data from the old mesh to the new mesh which can result in loss of accuracy.

A simpler method to simulate crack growth is the element deletion method wherein the crack is allowed to propagate in any direction and does not require re-meshing or the definition of new contact surfaces. Strong discontinuities in the field variable are not explicitly represented as the fractured elements are failed such that they can no longer sustain deviatoric or tensile volumetric stresses. Beissel *et al.* (1998) put forward an algorithm for element deletion for the finite element analysis of dynamic elastic-plastic fracture mechanics. Recently, Song *et al.* (2008) published a comparative study of extended finite element method (XFEM), element deletion method and inter-element crack method for dynamic crack propagation in brittle materials.

The idea to enrich the approximation field was introduced in the global-local analysis strategies. The general idea was to get a global solution using a coarse mesh of finite elements and accurate results were then found by focusing on the areas of interest, refining the mesh and using field variables from the global analysis as inputs for the refined mesh. The detailed (local) analysis was performed by assimilating known physical behaviours and/or analytical solutions (as boundary conditions) into the computational model to achieve convergence. Noor (1986) presented an assessment of the potential of different global-local analysis strategies for predicting the non-linear responses of structures. In a more recent application of global-local analysis strategies, Kim *et al.* (2008) presented an analysis of interacting cracks using a generalised finite element method (GFEM) enriched with global-local functions, where the global approximation space was enriched using the solutions of the local boundary value problems estimated in a global-local analysis.

Gifford and Hilton (1978) extended the finite element method by enriching the

field variable with the analytical solution for calculating the combined mode I and mode II stress intensity factor for axisymmetric and planar structures of arbitrary geometry and loading. The approximated displacement was taken to be a combination of the conventional FEM polynomial expression and an enrichment term such that $u = u_{std} + u_{enr}$. But, this enrichment reduced the sparsity of the stiffness matrix and required a higher order Gaussian quadrature for numerical integration. Also, the crack tip had to be defined specifically on the node of an element for this scheme to work.

Belytschko *et al.* (1988) developed a method by which localisation zones (thin bands of high strain in materials) were embedded (enriched) at an element level. This was achieved by altering the strain field within the framework of a three-field (displacement, strain and stress fields) variational principle. The strain is discontinuous across the interfaces between the localisation band and the remainder of the element, and the jump in strain field across the localisation band was found by imposing traction continuity and compatibility within the element. This methodology called the embedded finite element method (EFEM) was intended in cases where the localisation area was significantly smaller than the element size. This method reduces the dependence of the finite element method on mesh size and allows for approximations to be calculated by meshes which are not adjusted to the solutions prior to the calculations. Oliver (1996b) used EFEM to address the finite element approximation to the solution of the strong discontinuity problem (Oliver (1996a)). In this work, an additional discontinuous displacement field is incorporated into the finite element formulation within the framework of EFEM i.e. an approximation to the displacement jump is added to the standard element. Jirásek (2000) evaluated a number of techniques that enriched the standard finite element interpolation with additional terms corresponding to a displacement or strain discontinuity within a unified framework.

The enriched approximation of the field variable was expressed in a generic form as,

$$u \approx Nd + N_c d_c \tag{1.2}$$

$$\epsilon \approx Bd + Ge \tag{1.3}$$

$$\sigma \approx Ss \tag{1.4}$$

where N is the standard displacement interpolation matrix (containing the shape functions), B is the standard strain interpolation matrix (containing the derivatives of the shape functions), N_c and G are matrices carrying enrichment terms for displacement and strains respectively, S is the stress interpolation matrix, and vectors d_c, e and s are the enriched degrees of freedom and are unknown. In contrast, the extended finite element method (XFEM) also being a local enrichment scheme, instead uses the partition of unity (PUM) to incorporate an enrichment function into the field variable. A prominent aspect of employing PUM in XFEM is that it enforces the conformity of the global approximation space.

Dolbow and Belytschko (1999) proposed a new computational method called the extended finite element method (XFEM), aimed at correcting the above shortcomings by using conventional FEM to model cracks and other defects with discontinuous interfaces. XFEM made a significant improvement to the foundation of conventional FEM. In the last 17 years, XFEM has been continually improved and advanced, making it a powerful and promising method for treating discontinuous fields, localised deformation, fracture, etc. It is being widely used in civil engineering, aviation, material science etc.

The core idea of XFEM is to use a discontinuous function to capture the jump in field variables (e.g. displacement) in the computational domain. This way an arbitrary discontinuity can be added to the finite element function independent of the mesh. It is this advantage that makes it suitable for dealing with problems involving

defects. Another advantage of XFEM is that it uses known analytical solutions to construct the enrichment shape functions, so accurate results can be obtained. When applying conventional FEM to model defects containing singularities, a very dense mesh has to be used. However, in XFEM, by introducing known displacement solutions for the defects into the enrichment shape function, an acceptable solution can be derived for a relatively coarser mesh.

XFEM is not only used to model cracks, but also to model voids and inclusions. The difference is that for cracks, the discontinuous field is displacement whereas, for inclusion and voids, it is the strain. These two settings are defined as a strong discontinuity (jump in the displacement field) and a weak discontinuity (jump in the derivative of the displacement) respectively. Two different enrichment shape functions will have to be used to model the two different discontinuities.

The finite element method is based on mesh interpolation; low-quality meshes generate larger errors, require remeshing and may not be feasible in the case of three-dimensional models. Also, the classical mesh-based methods are not apt to solve models with discontinuities that do not align with the element boundary. Remeshing or discontinuous enrichment will need to be used to deal with moving discontinuities. However, remeshing is expensive, difficult in three dimensions and requires a transfer of quantities between consecutive meshes which in turn leads to a reduction in accuracy. A feasible alternative would be the extended finite element method (XFEM) which enriches the approximation space such that weak and strong discontinuities can be represented. Dependence on the mesh to formulate the approximation can also be eliminated with meshless methods (MM). The element-free Galerkin method (EFG) was one of the first meshless methods built on the global weak form. Using only nodal data, Belytschko *et al.* (1994) formulated the element-free Galerkin method for arbitrary shapes. The trial and test functions for the weak form were constructed

using moving least-squares interpolants. Least-squares approximation was first used to fit the interpolants (polynomial) to the nodal values in Nayroles *et al.* (1992)'s method to develop the Galerkin equations using only a mesh of nodes and a boundary description thus eliminating the need of a finite element mesh completely. Unless the weighting functions are singular, the moving least-squares method interpolants do not pass through the data as the interpolation functions are not equal to unity at the nodes. This works against the application of essential boundary conditions but is greatly outweighed by the benefits of eliminating elements and the consequent element meshing. Detailed review and applications on meshless methods can be found in review papers by Belytschko *et al.* (1996) and Nguyen *et al.* (2008).

Melenk and Babuška (1996) discussed the mathematical foundation of the partition of unity finite element method (PUFEM). They showed that PUFEM has the ability to include the partial differential equation being solved in the finite element space knowledge. PUFEM has been the basis of the extended finite element method. The basic idea was to include a non-smooth enrichment function, usually non-polynomial into the approximation using the partition of unity. This produces an enriched basis function which could be non-smooth and non-polynomial depending on the type of enrichment used. It is, therefore, possible to locally approximate the field variable with a non-smooth function. Belytschko and Fleming (1999) used the idea of PUM to expand the EFG basis with non-polynomial functions so as to successfully incorporate discontinuities in the approximation or the derivative of the approximation space within the framework of meshless methods.

The idea of modelling crack problems with minimal or no remeshing was developed by Belytschko and Black (1999). They added discontinuous functions to the finite element approximation to describe the boundary of the crack. This method enabled arbitrary alignment of the crack within the mesh, but it required remeshing

for severely curved cracks. The Haar function and an asymptotic near tip field for modelling crack growth by enrichment was introduced by Dolbow and Belytschko (1999). With the improved methodology, the entire crack could now be represented independently from the mesh, based on the construction of the enriched approximation. This method came to be known as the extended finite element method (XFEM). The next significant step was by Dolbow *et al.* (2000) in presenting a technique to model arbitrary discontinuities in the finite element framework by locally enriching a displacement based approximation using the partition of unity method and considering cracks and crack growth in two-dimensional elasticity and Mindlin-Reissner plates as specific examples. When the elements containing the crack surface and crack tip are enriched, some nodes have both the standard and enriched degrees of freedom. The elements containing these nodes (known as the blending elements) would decrease the efficiency of computation since they do not satisfy the partition of unity. XFEM was extended to model three-dimensional cracks by Sukumar *et al.* (2000). For three-dimensional crack modelling, a discontinuous function was used to model the interior of the crack surface and added to the finite element approximation within the context of a displacement based Galerkin formulation. Chessa *et al.* (2003) improved the performance of these elements by using a variant of the assumed strain method known as the enhanced strain method, which is based on the Hu-Washizu variational principle. The enrichment function in the blending domain introduces undesirable and additional terms; these terms were eliminated using the enhanced strain field. Extensions of finite element method for modelling cracks with multiple branches, multiple holes and cracks emanating from the hole were presented by Sukumar and Belytschko (2000).

The level set method (LSM) to represent the crack location, including the location of crack tips was coupled with the extended finite element method to model crack

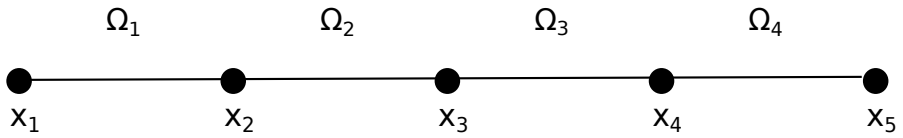

Figure 1.3: FEM discretization of the domain Ω.

growth by Stolarska *et al.* (2001). In modelling arbitrary discontinuities in finite elements, both discontinuities in the function and its derivatives were considered by Belytschko *et al.* (2001). Level sets were used to update the position of discontinuities by constructing the discontinuous approximation in terms of signed distance functions. Duflot (2007) published an overview of the representation of cracks with level set functions with additional and improvised methods of describing the level set functions for crack propagation problems in 2D and 3D.

Since the discontinuities can be arbitrarily aligned, independent of the mesh, within the framework of XFEM, holes and inclusions can also be easily modelled using XFEM. On the other hand, modelling holes and inclusions using the standard finite element method require the mesh to conform to the shape of holes and inclusions. The ease with which holes and inclusions could be modelled using XFEM was shown by Sukumar *et al.* (2001). Material interfaces in composites can also be modelled to predict the mechanical properties of the material using XFEM.

XFEM locally incorporates special functions describing the field behaviour into the finite element approximation. It is based on the partition of unity method and is able to completely capture all the features of the discontinuity. The following lines will illustrate the XFEM methodology using a 1-D model to locally enrich a field. The 1-D domain Ω, is discretized into sub-domains $\Omega_1, \Omega_2, \Omega_3, \Omega_4$. The coordinates of the nodes are $x_i = \{x_1, x_2, x_3, x_4, x_5\}$. We now associate each node with an interpolation function (or shape function) ϕ_i to help approximate the field. These shape functions have contact supports $\omega_i = \{\omega_1, \omega_2, \omega_3, \omega_4\}$, which correspond to the union of element

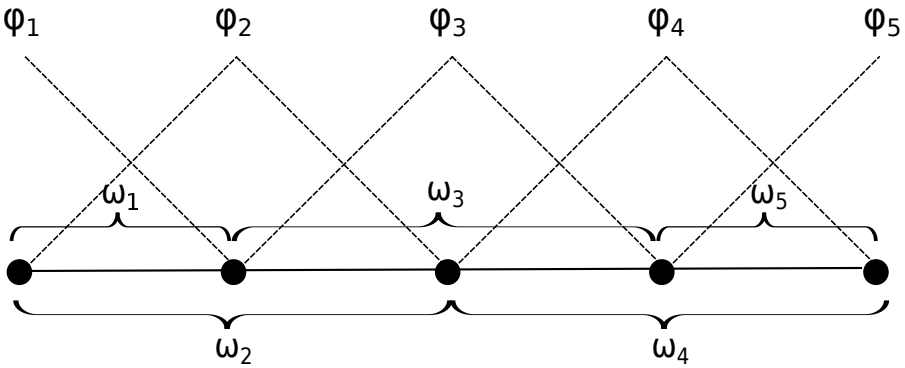

Figure 1.4: Interpolation functions.

sub-domains connected to node i. The corresponding FEM approximation is:

$$u^h(\mathbf{x}) = \sum_{i=1}^{5} \phi_i(\mathbf{x}) u_i \tag{1.5}$$

We now need to define a function to capture the local features of the discontinuity in order to approximate the field accurately; let $p(\mathbf{x})$ be the approximating function locally, that approximates the field u in the region of discontinuity. $p(\mathbf{x})$ could be defined as a Heaviside function $H(\mathbf{x})$ to represent the jump in the displacement field (one of many examples). We pick element Ω_3 to be enriched with the function $H(\mathbf{x})$ in the interval $[x_3, x_4]$. Consequently, the nodes associated with the supports Ω_3 and Ω_4 will be enriched. We then need to define the partition of unity functions in the region of interest. Since the standard finite element shape functions already possess the partition of unity property, they can be used as the interpolants ϕ_3 and ϕ_4 (any polynomial/non-polynomial function can be used as an interpolant as long as it satisfies eq. 1.6).

$$\sum_{i=1}^{n} \phi_i(\mathbf{x}) = 1 \tag{1.6}$$

The enrichment term can now be incorporated as

$$\sum_{j=3}^{4} \phi_j p(\mathbf{x}) a_j \tag{1.7}$$

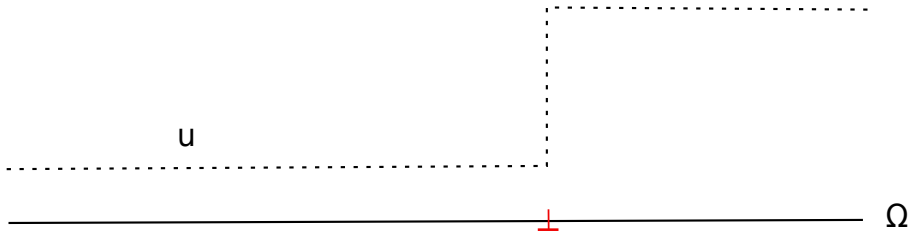

Figure 1.5: Discontinuity in the field u over Ω.

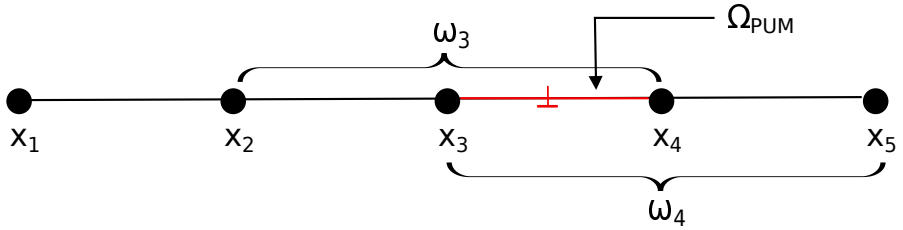

Figure 1.6: XFEM discretization of the domain Ω.

where a_j are the enriched degrees of freedom. The corresponding extended approximation of the standard FEM is

$$u^h(\mathbf{x}) = \sum_{i \in I} \phi_i u_i + \sum_{i \in J} \phi_i p(\mathbf{x}) a_i \tag{1.8}$$

where I is the set of all nodes, I $= \{x_1, x_2, x_3, x_4, x_5\}$ and J is the set of enriched nodes, J $= \{x_3, x_4\}$ with J $\subset$ I.

- when $i \in I$

$$u^h(\mathbf{x}_i) = \sum \phi_i u_i = u_i \tag{1.9}$$

This is a case of standard FEM where an approximation is in terms of the nodal values.

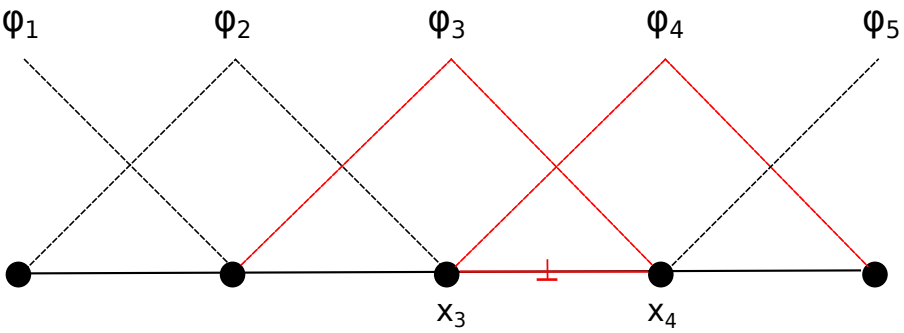

Figure 1.7: Standard FEM interpolation functions with additional PUM functions.

- when $i \in J$

$$u^h(\mathbf{x}_i) = \sum \phi_i u_i + \sum \phi_i p(\mathbf{x}_i) a_i = u_i + p(\mathbf{x}_i) a_i \tag{1.10}$$

Nodal interpolation is no longer a viable approximation, i.e $u(\mathbf{x}_i) \neq u_i$

Discontinuities arbitrarily aligned with the mesh can be modelled with the help of extended finite element method through the use of the partition of unity. Any function (typically non-polynomial) can be incorporated into the FEM approximations with the concept of partition of unity. The general concept includes defining functions whose sum is equal to one on the domain Ω^{PUM}, see eq. 1.6.

When using the partition of unity functions, it can be observed that

$$\sum_{i \in I} \phi_i p(\mathbf{x}) = p(\mathbf{x}) \tag{1.11}$$

where $p(\mathbf{x})$ is the local approximating function. This illustrates that any function multiplied with the partition of unity function can be exactly reproduced. It also inherits the smoothness of partition of unity function.

Let s_i be the space of functions by which the field $u^h|_{\omega_i}$ can be approximated well, the global space $u^h|_\Omega$ can be approximated with S such that

$$S = \sum \phi_i s_i \tag{1.12}$$

Owing to the characteristics of partition of unity functions (their sum is equal to 1 and their ability to reproduce any function), any function of any nature can be added to the local approximation space. The local approximation functions can be polynomial functions, non-polynomial functions, discontinuous functions (Heaviside, Delta, absolute value function), singular functions, trigonometric functions, logarithmic functions, or any function of known solution characteristics. We can now define the enriched functional space as $\{p_1(\mathbf{x}), p_2(\mathbf{x}), ...p_i(\mathbf{x})\}$. For example, in modelling

crack growth, at least two enrichment functions are used. For elements completely cut by the crack, Heaviside enrichment is used with the following enriched space of functions,

$$s_i = \{H(\mathbf{x})\} \tag{1.13}$$

For the element(s) containing the crack tip, at least one enrichment function obtained from the analytical solution employing linear elastic fracture mechanics (LEFM) is used. The corresponding enriched approximation space of functions is,

$$s_i = \{p(\mathbf{x})\} \tag{1.14}$$

We can then form the partition of unity basis functions by multiplying the standard finite element interpolation with the local enrichment functions,

$$\phi_{enr} = \phi_j p_k(\mathbf{x}) \tag{1.15}$$

where $j = 1\ to\ n_{enr}$, n_{enr} is the number of enriched nodes and $k = 1\ to\ n_{ENR}$, n_{ENR} is the number of enrichment functions for each enriched node. In general, any function that qualifies to be a partition of unity function can be used to obtain the enriched basis by multiplying it with the local approximating function (standard finite element shape functions are popularly used).

We can now write the extended finite element basis as,

$$\phi_i|_{i=1}^{nen} = \phi_{std} \cup \phi_{enr} \tag{1.16}$$

$$\phi_i|_{i=1}^{nen} = \phi_i|_{i=1}^{nen} \cup \{\phi_j p_1(\mathbf{x}), \phi_j p_2(\mathbf{x}), ...\phi_j p_k(\mathbf{x})\}|_{j=1}^{n_{enr}} \tag{1.17}$$

where nen is the total number of nodes in the domain.

Let the nodal shape functions for finite element method be defined by N, then the nodal shape function for extended finite element method would be,

$$\begin{bmatrix} N \end{bmatrix} = \begin{bmatrix} N_{std} & N_{enr} \end{bmatrix} \tag{1.18}$$

and the gradient of shape functions will be,

$$\left[B\right] = \left[B_{std} \quad B_{enr}\right] \tag{1.19}$$

An XFEM approximation (say displacement) can now be written as,

$$u_{XFEM} = \sum_{i=1}^{nen} N_i u_i + \sum_{j=1}^{n_{enr}} N_j \left(\sum_{k=1}^{n_{ENR}} p_k(\mathbf{x}) a_j \right) \tag{1.20}$$

$$u_{XFEM} = u_{std} + u_{enr} \tag{1.21}$$

In general,

$$u_{XFEM} = \left[N_{std} \quad N_{enr}\right] \begin{bmatrix} u_{std} \\ u_{enr} \end{bmatrix} \tag{1.22}$$

1.3 Introduction to Inclusions

The term 'inclusion' in the context of metallurgy and metal processing refers to the hard particles that enter or form in the liquid metal during the melt stage of processing which are eventually trapped when the melt solidifies. These hard particles could act as a crack propagator or as a region of high stress intensity. A dislocation in the vicinity of such an inclusion experiences attractive or repulsive force depending on the difference in the material properties of the inclusion and the matrix containing the dislocation. A harder inclusion will tend to repel a dislocation while a softer one will attract it. In alloys, dislocations may either interact with atoms that replace atoms comprising the metallic crystals in case of substitutional alloys or they may interact with atoms trapped in the spaces between the atoms of the crystal matrix in case of interstitial alloys.

The force on a dislocation interacting with inhomogeneity was first examined by Head (1953b), by considering an infinite elastic medium of shear modulus G_1 for $x > 0$, and G_2 for $x < 0$, with a dislocation running parallel to the interface.

He concluded that the dislocation was simply either attracted or repelled by the inhomogeneity. These results were later used by Fleischer (1960) to study the effect of non-uniformities on the hardening of crystals. The effect of changes in elastic modulus and lattice parameter on the ease with which a dislocation can move in a crystal was examined. This paper concluded that dislocations that cross into a region of different lattice constant create immobile dislocations at the interface and that the interface dislocations which exist at a free surface will result in surface hardening. Sendeckyj (1970) considered a screw dislocation '1' near an elastic elliptic cylindrical inclusion '2' and observed that a hard inclusion ($K > 0$ i.e. $\mu_2 > \mu_1$) would repel the dislocation, while a soft one ($K < 0$ i.e. $\mu_2 < \mu_1$) would attract it.

$$K = \frac{\mu_2 - \mu_1}{\mu_2 + \mu_1} \tag{1.23}$$

where μ is the shear modulus.

Dundurs and Mura (1964) showed that the interaction between a dislocation and an inclusion was not limited to either simply an attraction or a repulsion but that the dislocation was under stable equilibrium at a finite distance from the interface. They considered the interaction energy to be minimum at the stable equilibrium position in an attempt to the study the motion of dislocations near inhomogeneities. Their results indicated that the interaction was affected by material constants to a large extent, particularly on the difference in Poisson's ratios in addition to the difference in shear moduli of the inclusion and the matrix containing the dislocation.

Nicholson *et al.* (1960) examined thin foils of aluminium alloys using transmission electron microscopy wherein dislocations were introduced in the alloys by rolling before thinning. These dislocations were observed to move under the effect of thermally induced stresses. The interactions between the dislocations and precipitates showed that the dislocations pass through zones, coherent and partially coherent pre-

cipitates but avoid incoherent precipitates. Dislocations with high mobility inside manganese sulphide inclusions in steel were discovered during a study of the effect of non-metallic inclusions on the weldability of steel by Boniszewski and Baker (1963). Considering these observations and with an intend to pursue further the study by Dundurs and Mura (1964), Dundurs and Sendeckyj (1965) observed the behaviour of an edge dislocation situated inside an inclusion within the framework of the classical theory of elasticity. The conditions under which the centre of the inclusion is a stable equilibrium position for the dislocation were given and it was also established that the equilibrium positions away from the centre are unstable. The results showed that the difference in material constants contributed significantly towards the above conclusion.

Fukuzaki and Shioya (1986) and Fukuzaki and Shioya (1987) in their studies on the interaction between an edge dislocation and two circular inclusions in an infinite medium arranged the edge dislocation on the axis of symmetry of the two inclusions in the order of inclusion-inclusion-edge dislocation and inclusion-edge dislocation-inclusion respectively. The results showed that the interaction was considerably affected by the geometrical relations and combination of elastic constants of the inclusions and dislocation involved. It was shown that the dislocation had a stable equilibrium position or an unstable equilibrium position at some distance from the inclusions defined by the combination of elastic constants. They observed that the force on the dislocation increased as the dislocation approached the inclusions, and that the force with which it was attracted to or repelled by the inclusion depended heavily on the difference in elastic constants of the inclusion and the matrix containing the dislocation.

Arsenault and Fisher (1983) suggested that the increased strength of Al-SiC composites could be explained by the occurrence of high dislocation density in the alu-

minium matrix. This study found at least three Burgers vector at any given location. The large difference (10 : 1) in the coefficients of thermal expansion of aluminium and SiC was seen as the driving mechanism for the dislocation generation of such high density. When the composite is cooled from high temperatures in the action of processing, misfit strains large enough to generate dislocations are induced as a result of differential thermal contraction at the Al-SiC interface. In a different study by Chawla and Metzger (1972) of Cu-W composites using etch-pitching studies, a high dislocation density at the Cu-W interface reduced with increasing distance from the interface. A difference (4 : 1) in coefficients of thermal expansion of copper and tungsten caused the dislocations to materialise. Dislocations may also be introduced into composites during plastic deformation process of manufacturing such as extrusion or dislocations may not be completely removed but trapped by the composite constituents, resulting in high dislocation density even after annealing. Arsenault and Shi (1986) cooled Al-SiC composites from annealing temperatures to observe dislocations at the Al-SiC interface. This study noted that the intensity of dislocation generation at the Al-SiC interface was related to the size and shape of SiC particles with the intensity being low for small and nearly spherical particles. Also, thermal cycling caused the dislocations to disappear at high temperatures and reappear at the Al-SiC interface and precipitates on cooling.

1.4 Why Is This Study Useful?

Mechanical properties of materials are considerably affected by the defects in them. These defects need to be modelled and the cost of these computations is usually very high with a limiting factor on the model size. Hence, the formulation of computationally efficient models is needed. In a continuum-based approach, the analytical infinite domain solutions and image stress fields need to be superimposed

to obtain the total stress field. A finite element model with boundary conditions to cancel the effect of the infinite domain dislocation fields will have to be chosen to obtain the solution. For a dislocation core close to a boundary, a large number of integrations points are needed to estimate the total stress field accurately. Also, the cost of these computations increases with increase in the number of dislocations as the infinite domain fields and image stress fields would have to superimposed for each dislocation. In these models, the image stress is only approximately calculated from analytical equations that are applicable only to simple boundary geometries. Additionally, selecting boundary conditions to exactly cancel the effect of the infinite domain dislocation fields is difficult and this was shown by Devincre *et al.* (2001). Methods based on superposition are difficult to apply to problems involving anisotropy and material interfaces. Besides, the standard FEM is only able to capture the slip across the glide plane in an average sense and is, therefore, unable to represent the discontinuity in a field variable within a single element.

A method which does not depend on the analytical solution, does not use superposition or require the calculation of image stresses is therefore needed. XFEM allows arbitrary discontinuities to be modelled in the framework of the finite element mesh. An arbitrary discontinuity can be introduced into a finite element solution without the need for it to conform to the mesh in any way. The ease with which arbitrary discontinuities can be modelled with XFEM is its principal benefit to this study. The slip across the glide plane can be modelled exactly within a single element within the framework of XFEM. This method can be extended to anisotropic materials and to easily solve problems involving interfaces. XFEM is not to replace the superposition methods but to solve problems involving material interfaces more efficiently, which is difficult for existing methods.

Foreign atoms in solid solutions, precipitates in alloys and other kinds of inhomo-

geneities play an important role in determining the mechanical properties of materials because of their interaction with dislocations. In this study, some aspects of the interaction between the larger scale inhomogeneities and dislocation have been analysed by considering an edge dislocation in the vicinity of impenetrable inclusions whose elastic properties are different from those of the matrix containing the dislocation. Dislocations in composites may materialise during cooling from high annealing or processing temperatures due to differential thermal contraction of the constituents involved. The interaction of these dislocations generated at the interfaces with the precipitates will dictate the mechanical properties of the composite in the form of increased strength of the matrix in the Al-SiC composite for example. It is therefore of interest to model the interactions between dislocations and inclusions using a computationally more efficient method.

Chapter 2

NUMERICAL METHOD

2.1 Problem Formulation

Consider a body with domain Ω bounded by Γ with tractions $\bar{\mathbf{t}}$ defined on the boundary Γ_t. Displacement boundary conditions are applied at the boundary surface Γ_u allowing us to write $\Gamma = \Gamma_t \cup \Gamma_u$. In addition, the body contains an internal discontinuity, a dislocation $\perp$ denoted by $\Gamma_\perp$. The corresponding scenario is illustrated in fig. 2.1.

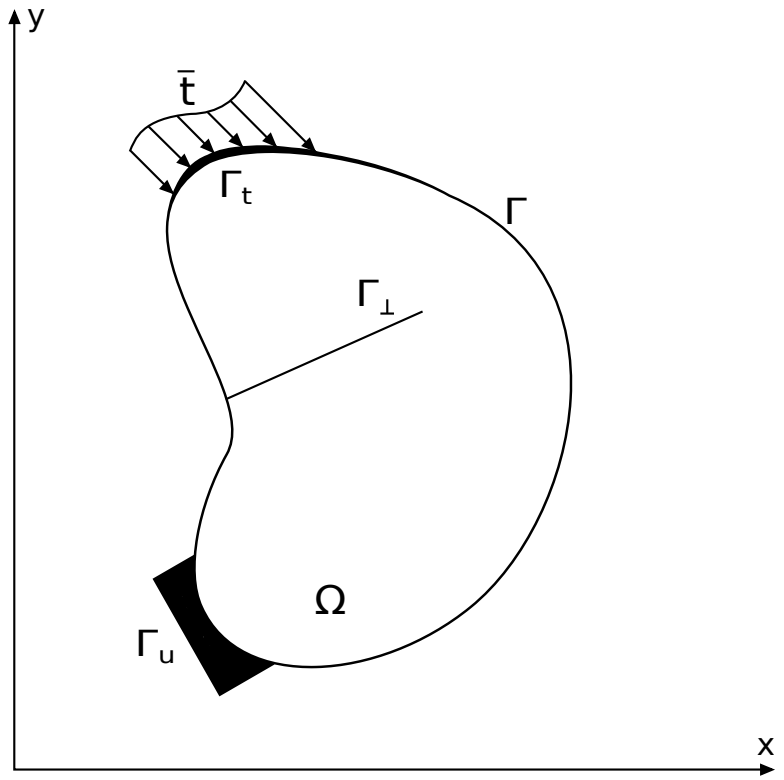

Figure 2.1: Domain definition and notation.

The strong form of the equilibrium equation is,

$$\nabla \cdot \sigma + b = 0 \tag{2.1}$$

The boundary conditions for the domain Ω are,

$$\sigma \cdot n = \bar{t} \quad \text{on} \quad \Gamma_t \tag{2.2}$$

$$\sigma \cdot n = 0 \quad \text{on} \quad \Gamma_\perp \tag{2.3}$$

$$u = \bar{u} \quad \text{on} \quad \Gamma_u \tag{2.4}$$

where n is the outward unit normal and σ is the cauchy stress tensor.

Adopting a small strain and linear elastic formulation, the strain-displacement relation can be expressed as,

$$\epsilon = \nabla_s u \tag{2.5}$$

where ϵ is the strain tensor and $\nabla_s u$ is the symmetric part of the displacement gradient.

The constitutive equation as per Hooke's law is,

$$\sigma = \mathbb{C} : \epsilon \tag{2.6}$$

where $\mathbb{C}$ is the elastic material stiffness tensor.

The space of admissible displacement field is given as,

$$u \in U = \{u \in C^0, u = \bar{u} \text{ on } \Gamma_u, u \text{ is discontinuous on } \Gamma_\perp\} \tag{2.7}$$

and the test function is given as,

$$w \in W = \{w \in C^0, w = 0 \text{ on } \Gamma_u, w \text{ is discontinuous on } \Gamma_\perp\} \tag{2.8}$$

The weak form of the equilibrium equation is now given as,

$$\int_\Omega \epsilon(w)^T : \sigma(\epsilon(u)) \, \mathrm{d}\Omega - \int_\Omega g \cdot w \, \mathrm{d}\Omega - \int_{\Gamma_t} \bar{t} \cdot w \, \mathrm{d}\Gamma = 0 \tag{2.9}$$

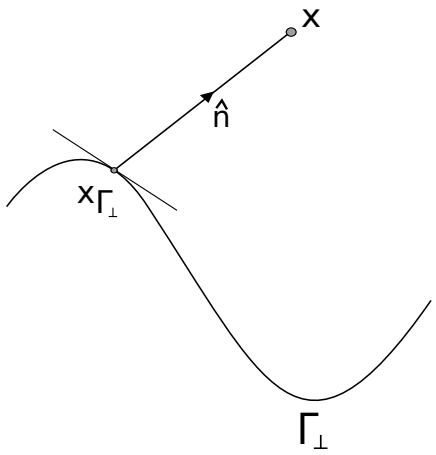

Figure 2.2: Signed distance function.

2.2 Level Set Representation of Discontinuities

Osher and Sethian (1988) introduced the level set method for tracking moving interfaces. The main idea of the level set method is to represent the interfaces at any time t, with a zero level set function i.e $\phi(\mathbf{x}, t) = 0$, where $\phi(\mathbf{x}, t)$ is the level set function.

For modelling a dislocation, the level set function is taken as a signed distance function such that the level set function has positive values on one side of the interface and negative values on the other side of the interface and the interface is represented by the zero level set function. As the dislocation is a discontinuity that does not divide the domain into two distinct parts entirely, we define two level set functions to fully characterise the dislocation, (i) a normal level set function f and (ii) a tangential level set function g. Both the level set functions are defined as signed distance functions.

For determining the signed distance functions, let $\Gamma_\perp$ represent a dislocation $\perp$. Then for an arbitrary point $\mathbf{x}$, we find a point $\mathbf{x}_{\Gamma_\perp}$ on the discontinuity such that $|\mathbf{x} - \mathbf{x}_{\Gamma_\perp}|$ is minimum. We then define a unit vector $\hat{n}$, normal to the discontinuity at $\mathbf{x}_{\Gamma_\perp}$. The signed distance function is then represented as:

$$f(\mathbf{x}) = (\mathbf{x} - \mathbf{x}_{\Gamma_\perp}) \cdot \hat{\mathbf{n}} \tag{2.10}$$

Eq. 2.10 is the normal level set function. The tangential level set function is calculated by determining the minimum signed distance function to the normal at the discontinuity. The signed distance function corresponding to the tangential level set function is,

$$g(\mathbf{x}) = (\mathbf{x} - \mathbf{x}_{\Gamma_\perp}) \cdot \hat{\mathbf{t}} \tag{2.11}$$

where $\hat{t}$ is the normal to the normal at the discontinuity. The dislocation can now be fully characterised by the two level set functions f and g such that $f = 0$ and $g < 0$ on the glide plane. The dislocation core can be identified by the intersection of the normal and tangential zero level set functions i.e intersection of $f = 0$ and $g = 0$. Formally we can write this as:

$$\begin{aligned} \Gamma_\perp &= \{\vec{\mathbf{x}} \in \mathbb{R} : f(\vec{\mathbf{x}}) = 0 \ \cap \ g(\vec{\mathbf{x}}) \leq 0\} \\ \partial\Gamma_\perp &= \{\vec{\mathbf{x}} \in \mathbb{R} : f(\vec{\mathbf{x}}) = 0 \ \cap \ g(\vec{\mathbf{x}}) = 0\} \end{aligned} \tag{2.12}$$

The level set functions are computed over the entire domain. Within the rest of the domain f, will have a positive value above the glide plane and a negative value below the glide plane. The function g, on the other hand, will have a positive value to the right of the normal at the dislocation core and negative values on the left of the normal to the dislocation core.

Within the framework of finite element method, the level set functions f and g defined above can be interpolated within an element using the standard finite element shape functions as:

$$\phi(\mathbf{x}) = N_i(\mathbf{x})\phi_i \tag{2.13}$$

where ϕ_i are the values of the level set functions at the nodes.

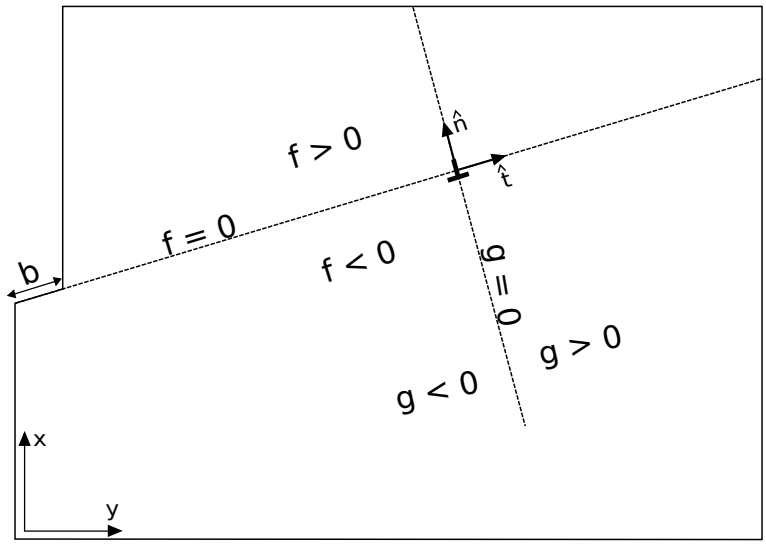

Figure 2.3: Description of an edge dislocation using level set functions $f(\mathbf{x})$ and $g(\mathbf{x})$. $\mathbf{b}$ is the Burgers vector.

Furthermore, within the framework of XFEM, the level set functions can also be employed to determine the Heaviside enrichment function. We can define an enrichment function H as:

$$H = \begin{cases} +1, & \phi > 0 \\ 0, & \phi < 0 \end{cases} \tag{2.14}$$

Issues with Modelling Dislocations Using the Level Set Method

The Level set method offers an elegant way of modelling discontinuities. Modelling discontinuities using level set functions within the framework of XFEM was first used by Stolarska *et al.* (2001). These functions can be used to identify the elements through which the glide plane passes as well as the element containing the dislocation. The elements cut by the glide plane can be found by:

$$f_{min} * f_{max} < 0 \quad \text{AND} \quad g_{max} < 0 \tag{2.15}$$

In cases where the glide plane passes through or very close to a node, incorrect

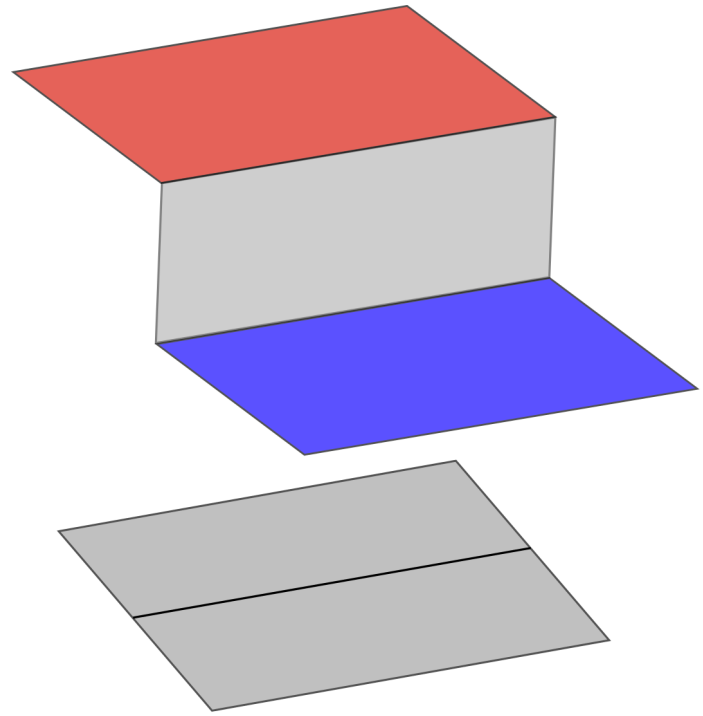

Figure 2.4: Heaviside function for an element completely cut by the glide plane of the dislocation.

enrichment is obtained. This is corrected by modifying the signed distance functions. If the signed distance function for a particular node is less than $\frac{1}{100}^{th}$ of the element size, it is set to be equal to $\frac{1}{100}^{th}$ of the element size. This effectively shifts the glide plane, forming a slight kink in it around the node. Algorithm 1 describes the concept used.

Algorithm 1 Shift glide plane around nodes

```
1: Compute element size.
2: Cut-off distance = 1% of element size.
3: for each node do
4:     if f ≤ cut-off distance then
5:         f = cut-off distance
6:     return false
7: end for
```

The next issue lies in the element containing the dislocation core. $g_{max} < 0$ in eq. 2.15 is not sufficient to determine the element containing the dislocation core. In

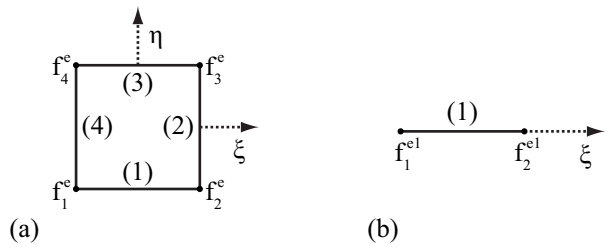

Figure 2.5: Parent element signed distance function values. Element edge numbers are indicated in parentheses.

such a case, algorithm 2 in addition to eq. 2.15 is adopted.

Algorithm 2 Enrich element containing the dislocation

```
for each node in element do
    if g_min < 0 then
        for each element edge do
            if f_1^e · f_2^e < 0 then
                Compute ξ_0 = (f_1^e + f_2^e)/(f_1^e − f_2^e)
                Compute g(ξ_0) = (1/2)(1 − ξ) g_1^e + (1/2)(1 + ξ) g_2^e
                if g(ξ_0) < 0 then
                    return true
            return false
        end for
    return false
end for
```

2.3 Dislocation Enrichments

Theoretically, the basic idea of the XFEM is to superimpose one or many enrichment terms to the conventional continuous interpolation. Enrichment terms involved in the approximated quantities are vital for describing any discontinuity. Discontinuities occurring in heterogeneous materials and structures are of two types (see fig 2.6): strong discontinuities, where there is a jump in the physical field and weak discontinuities where there is a jump in the gradient of the physical field. Enrichment functions are accordingly classified into two types. Functions corresponding to the first type are discontinuous and are used to describe strong discontinuities: the Heaviside function is popularly used in literature. Fries (2008) suggested that the sign step function

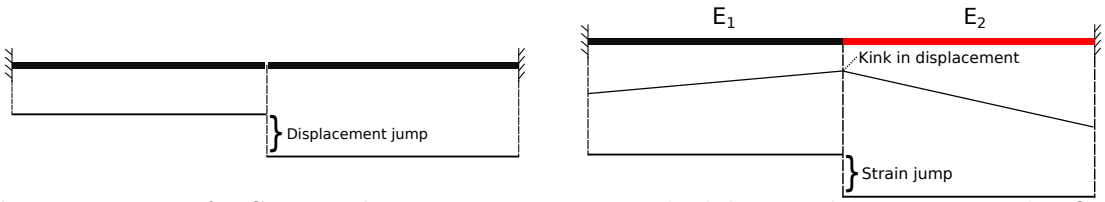

Figure 2.6: Left, Strong discontinuity in a cracked bar with a jump in the field variable. Right, Weak discontinuity in a bi-material bar with a jump in the gradient of the field variable.

can provide the same approximation as the Heaviside function. Functions used to model weak discontinuities are continuous, but their derivatives are not. Hansbo and Hansbo (2004) developed a method for modelling both strong and weak discontinuities; the approximation was constructed using two different independent fields. In this method, the crack properties were obtained by overlapping elements instead of involving additional degrees of freedom. The additional element was superimposed on the element cut by the discontinuity in order to construct the enriched field. Later, Areias and Belytschko (2006) commented that the Hansbo-Hansbo method can be derived using a linear combination of XFEM basis of the Heaviside type.

Incompatible Enrichment

An edge dislocation $\perp$ is described by a glide plane, a core and a Burgers vector, b. The glide plane is a strong discontinuity with a jump in magnitude equal to the Burgers vector in the displacement field. For an edge dislocation, the Burgers vector is tangential to the glide plane. Implementing the Volterra model of dislocations, the jump along the glide plane is inserted by adding an internal discontinuity to the displacement field. The displacement approximation with incompatible enrichment for an edge dislocation with Burgers vector b has the following form,

$$\mathbf{u}^h(\mathbf{x}) = \sum_{I \in nen} N_I(\mathbf{x})\mathbf{u}_I + b \sum_{J \in n_{enr}} N_J(\mathbf{x}) H(f(\mathbf{x}))H(g(\mathbf{x})) \tag{2.16}$$

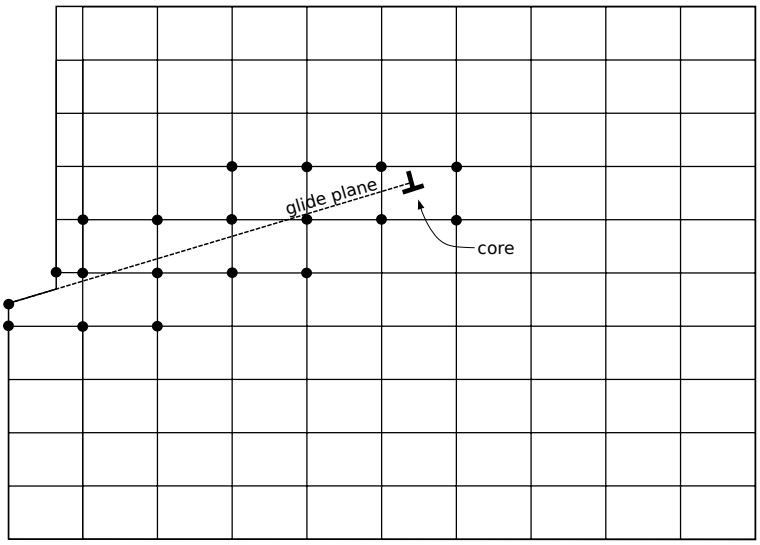

Figure 2.7: Description of the enrichment scheme. Dashed line depicts the glide plane and the black dots represent the nodes that are enriched.

where nen is the set of all nodes, n_{enr} is the set of enriched nodes, N_I and N_J are the standard finite element shape functions, $\mathbf{u}(\mathbf{x})$ are the nodal displacement degrees of freedom, $f(\mathbf{x})$ is the function defined by eq. 2.10 that describes the glide plane, $g(\mathbf{x})$ is the function defined by eq. 2.11 that describes the location of the core $\perp$ and $H(\mathbf{z})$ is the Heaviside function given by eq. 2.14. The nodes that are enriched, i.e those in the set n_{enr} are shown in fig. 2.7.

The form of enrichment terms in the displacement approximation eq. 2.16 is not suitable for imposing essential boundary conditions as the approximation loses its Kronecker-delta property. As the nodal displacement is now a function of both the standard and the enriched degrees of freedom, the enrichment functions need to be shifted such that they vanish at the nodes. Each enrichment function is shifted by a constant, as suggested by Belytschko *et al.* (2001) and Ventura *et al.* (2005). The shifted approximation is,

$$\mathbf{u}^h(\mathbf{x}) = \sum_{I \in nen} N_I(\mathbf{x})\mathbf{u}_I + b \sum_{J \in n_{enr}} N_J(\mathbf{x})\big[H(f(\mathbf{x}))H(g(\mathbf{x})) - H(f(\mathbf{x}_J))H(g(\mathbf{x}_J))\big] \tag{2.17}$$

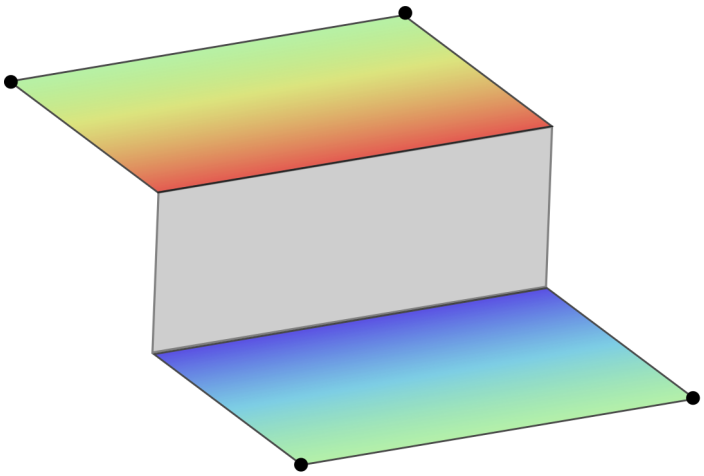

Figure 2.8: Magnitude of enrichment at element faces. Shifting the enrichment function causes the enrichment to disappear at the nodes (dots).

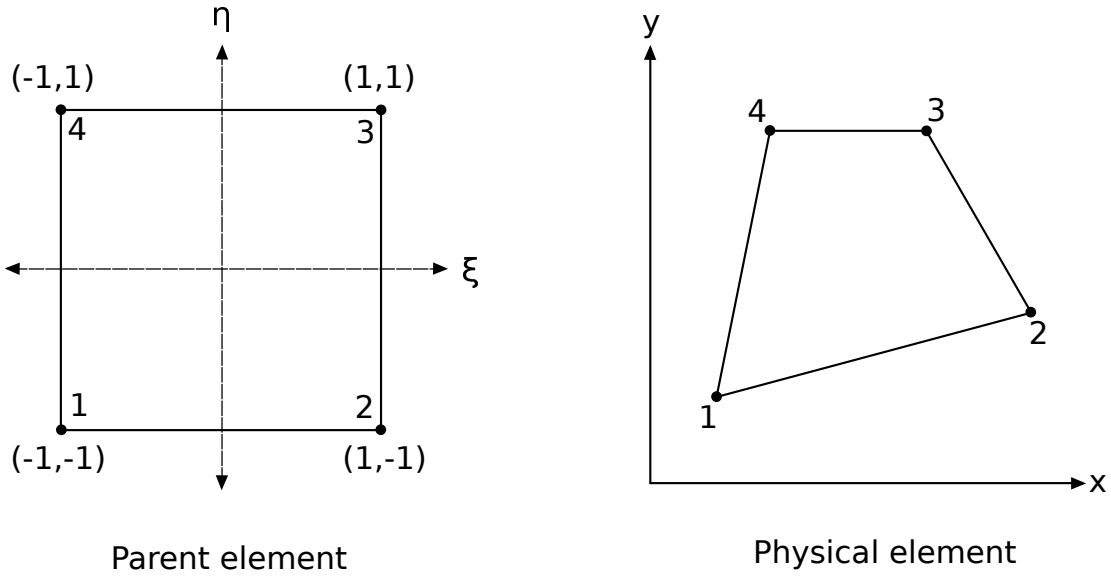

Figure 2.9: A four-node quadrilateral element.

2.4 Shape Functions

For a four noded isoparametric quadrilateral element, the standard finite element shape functions associated with each node are given as (Zienkiewicz *et al.* (1977)),

$$N_1 = \frac{1}{4}(1-\xi)(1-\eta) \tag{2.18}$$

$$N_2 = \frac{1}{4}(1+\xi)(1-\eta) \tag{2.19}$$

$$N_3 = \frac{1}{4}(1+\xi)(1+\eta) \tag{2.20}$$

$$N_4 = \frac{1}{4}(1-\xi)(1+\eta) \tag{2.21}$$

The corresponding displacement approximation is,

$$u(\mathbf{x}) = \begin{bmatrix} N_1 & 0 & N_2 & 0 & N_3 & 0 & N_4 & 0 \\ 0 & N_1 & 0 & N_2 & 0 & N_3 & 0 & N_4 \end{bmatrix} \begin{bmatrix} u_{x1} \\ u_{y1} \\ u_{x2} \\ u_{y2} \\ u_{x3} \\ u_{y3} \\ u_{x4} \\ u_{y4} \end{bmatrix} = N_{std}^{4Q} \mathrm{d}^e \tag{2.22}$$

where d^e is the nodal displacement matrix of an element. For an arbitrary enrichment function $p(\mathbf{x})$, the enriched shape function matrix is,

$$N_{enr} = \begin{bmatrix} N_1 p(\mathbf{x}) & 0 & N_2 p(\mathbf{x}) & 0 & N_3 p(\mathbf{x}) & 0 & N_4 p(\mathbf{x}) & 0 \\ 0 & N_1 p(\mathbf{x}) & 0 & N_2 p(\mathbf{x}) & 0 & N_3 p(\mathbf{x}) & 0 & N_4 p(\mathbf{x}) \end{bmatrix} \tag{2.23}$$

Knowing the shape functions and their gradients, the discretized gradient operator is,

$$B_{std} = \begin{bmatrix} N_{1,x} & 0 & N_{2,x} & 0 & N_{3,x} & 0 & N_{4,x} & 0 \\ 0 & N_{1,y} & 0 & N_{2,y} & 0 & N_{3,y} & 0 & N_{4,y} \\ N_{1,y} & N_{1,x} & N_{2,y} & N_{2,x} & N_{3,y} & N_{3,x} & N_{4,y} & N_{4,x} \end{bmatrix} \tag{2.24}$$

and the enriched discretized gradient operator is,

$$B_{enr} = \begin{bmatrix} (N_1 p)_{,x} & 0 & (N_2 p)_{,x} & 0 & (N_3 p)_{,x} & 0 & (N_4 p)_{,x} & 0 \\ 0 & (N_1 p)_{,y} & 0 & (N_2 p)_{,y} & 0 & (N_3 p)_{,y} & 0 & (N_4 p)_{,y} \\ (N_1 p)_{,y} & (N_1 p)_{,x} & (N_2 p)_{,y} & (N_2 p)_{,x} & (N_3 p)_{,y} & (N_3 p)_{,x} & (N_4 p)_{,y} & (N_4 p)_{,x} \end{bmatrix} \tag{2.25}$$

When $p(\mathbf{x})$ is the Heaviside function $H(x)$, the derivative of the enrichment term will be,

$$(N_I H)_{,x} = N_{I,x} H \tag{2.26}$$

2.5 Stiffness Matrix

The approximated displacement using a single enrichment function $p(\mathbf{x})$ can be expressed from eq. 1.20 as,

$$u_{XFEM} = \sum_{i=1}^{nen} N_i u_i + \sum_{j=1}^{n_{enr}} N_j p(\mathbf{x}) a_j \tag{2.27}$$

The corresponding strain approximation is,

$$\epsilon = \nabla^s N_i u_i + \nabla^s (N_j p(\mathbf{x})) a_j \tag{2.28}$$

where ∇^s is the symmetric gradient operator.

Using eq. 2.6, the stress approximation will then be,

$$\begin{aligned} \sigma &= \left[\mathbb{C}\right]\left[\nabla^s N_i u_i + \nabla^s (N_j p(\mathbf{x})) a_j\right] \\ &= \left[\mathbb{C}\right]\left[B_{std} u_i + B_{enr} a_j\right] \end{aligned} \tag{2.29}$$

where $B_{std} = \nabla^s N_i$ and $B_{enr} = \nabla^s (N_j p(\mathbf{x}))$ as discussed earlier.

Substituting these approximations into the weak form of the equilibrium equation (eq. 2.9) which is the standard principle of virtual work,

$$\int_{\Omega/\Gamma_\perp} \epsilon^T \sigma \, \mathrm{d}\Omega = \delta x F \tag{2.30}$$

$$\begin{Bmatrix} \delta u_i \\ \delta a_j \end{Bmatrix} \int_{\Omega/\Gamma_\perp} \begin{bmatrix} B_{std} \\ B_{enr} \end{bmatrix} \begin{bmatrix} \mathbb{C} \end{bmatrix} \begin{bmatrix} B_{std} u_i & B_{enr} a_j \end{bmatrix} \mathrm{d}\Omega = \begin{Bmatrix} \delta u_i \\ \delta a_j \end{Bmatrix} \begin{bmatrix} f^{ext} \\ f^{glide} \end{bmatrix} \tag{2.31}$$

$$\int_{\Omega/\Gamma_\perp} \begin{bmatrix} B_{std}^T \mathbb{C} B_{std} & B_{std}^T \mathbb{C} B_{enr} \\ B_{enr}^T \mathbb{C} B_{std} & B_{enr}^T \mathbb{C} B_{enr} \end{bmatrix} \begin{bmatrix} u_i \\ a_j \end{bmatrix} \mathrm{d}\Omega = \begin{bmatrix} f^{ext} \\ f^{glide} \end{bmatrix} \tag{2.32}$$

$$\begin{bmatrix} K_{uu} & K_{ub} \\ K_{ub}^T & K_{bb} \end{bmatrix} \begin{bmatrix} u \\ a \end{bmatrix} = \begin{bmatrix} f^{ext} \\ f^{glide} \end{bmatrix} \tag{2.33}$$

where $u = \begin{bmatrix} u_1, u_2 ..... u_{nen} \end{bmatrix}$ are the standard nodal degrees of freedom and nen is the number of nodes. The vector $a = \begin{bmatrix} a_1, a_2, ... a_{n_{enr}} \end{bmatrix}$ is the degrees of freedom associated with the enriched nodes and f^{glide} is the vector of reaction forces along the glide plane. The other terms are,

$$K_{uu} = \int_{\Omega/\Gamma_\perp} B_{std}^T \mathbb{C} B_{std} \, \mathrm{d}\Omega \tag{2.34}$$

$$K_{ub} = \int_{\Omega/\Gamma_\perp} B_{std}^T \mathbb{C} B_{enr} \, \mathrm{d}\Omega \tag{2.35}$$

$$K_{bb} = \int_{\Omega/\Gamma_\perp} B_{enr}^T \mathbb{C} B_{enr} \, \mathrm{d}\Omega \tag{2.36}$$

$$f^{ext} = \int_{\Omega} N^T g \, \mathrm{d}\Omega + \int_{\Gamma_t} N^T t \, \mathrm{d}\Gamma \tag{2.37}$$

The Burgers vector b defining the slip is assumed to be given, so its effect appears in the discrete equations as an additional force. The nodal displacements are obtained using eq. 2.33 and are given by,

$$u = K_{uu}^{-1}(f^{ext} - K_{ub} a) \tag{2.38}$$

The dislocations are now represented in eq. 2.38 by nodal forces $K_{ub}a$. The stiffness matrix K_{uu} is independent of the location and geometry of the dislocation and therefore does not change for a given mesh as the dislocation moves, whereas the nodal forces, $K_{ub}a$ will vary. Note that the discrete equations in eq. 2.38 are the standard

finite element equations and the effect of the dislocation manifests completely in the form of external forces, i.e the right-hand side of the equation. Accordingly, the proposed XFEM method can be effortlessly incorporated into a standard finite element software. Additionally, the stiffness matrix needs to be inverted only once and all ensuing steps would only involve the cheaper alternative of back-substitution.

Application of Displacement Boundary Conditions

Boundary conditions are imposed in a way similar to as they would be in a standard finite element method, i.e by constraining the nodal degrees of freedom. Through shifting in eq. 2.17, a node on the boundary of the domain, denoted as x_B will be bereft of enrichment. Effectively, the nodal displacements at x_B are $u(x_B) = u_B$, or the standard FEM. Specific displacements along a boundary are applied by constraining specific u_B in the solution of eq. 2.38. In the case of a free surface, no u_B will need to be altered, as the homogeneous natural boundary conditions follow directly from the weak form. In the case of a fixed boundary, the constraint $u_B = 0$ along the desired direction must be applied. Attention must be given to when the dislocation glide plane intersects boundaries where displacement boundary conditions are to be applied. To check if the necessary boundary conditions are imposed, the displacement of nodes on the boundary may be inspected.

2.6 Peach-Koehler Force

Peach and Koehler (1950) showed that the force F exerted on a line element ξds of a dislocation with a Burgers vector b by a stress σ is given by,

$$F = -\xi \times (\sigma \cdot b) \ \mathrm{d}s \tag{2.39}$$

where ξ is the local line tangent direction at the point on the dislocation line where the force is calculated. The cross product ensures that the Peach-Koehler force is always perpendicular to the line itself. The importance of the Peach-Koehler formula is that the force experienced by a dislocation is completely defined by the local stress σ on the dislocation, regardless of the origin of said stress. Local stresses can be induced by nearby dislocations or any other strain producing defects in addition to the surface traction forces. Using the superposition method, the stress σ on the dislocation is given by,

$$\sigma_{ij} = \sigma_{ij}^{\infty} + \sigma_{ij}^{image} \tag{2.40}$$

where σ_{ij}^{∞} is the stress on a dislocation in an infinite medium (or self-stress) and σ_{ij}^{image} is the image stress field due to the boundary of a finite body. The image stress can be calculated by solving the boundary value problem such that the surface traction $\sigma_{ij}^{image} n_j$ cancels the original traction $\sigma_{ij}^{\infty} n_j$ on the surface, where n_j is the component of normal vector to the surface. The self-stress can be calculated using the analytical infinite domain solutions.

Using the finite element solution of eq. 2.38 to compute the stresses needed to employ the superposition method is not accurate as the proposed method computes the total stress field which requires a greater mesh refinement at the core to achieve decent accuracy. Instead, image field methods like those described in Van der Giessen and Needleman (1995) may be more suitable.

Eshelby (1951) conceptualised that the force related to a singularity can be estimated as an integral over a surface enclosing it. This integral consists of the elastic field terms related to the singularity in an infinite medium multiplied by the difference between these terms and those actually involved. The expression for force is of the same form irrespective of its source. The force being estimated can be due to applied surface tractions, the presence of a free surface of a body or other singularities. In

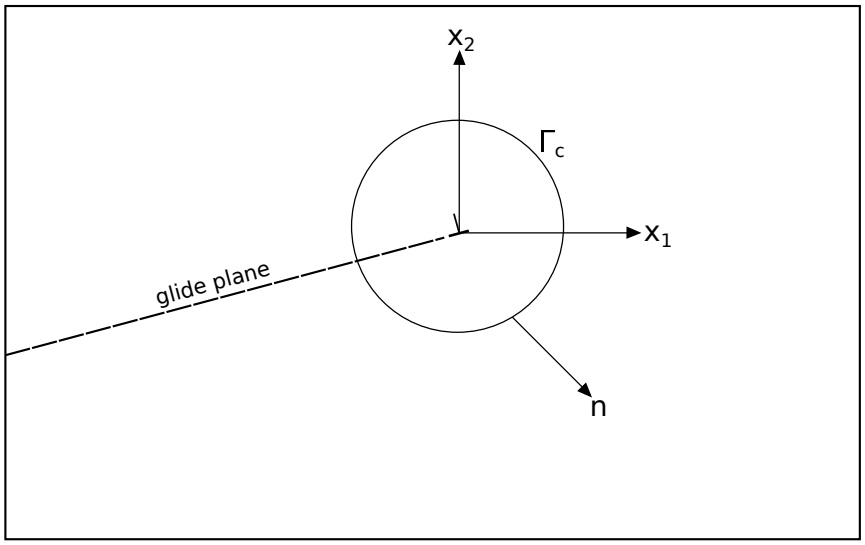

Figure 2.10: Conventions for calculation of the Peach-Koehler force from the J-integral.

this method, Eshelby's energy-momentum tensor is integrated over a closed contour around the dislocation core. Eshelby called this force a configurational force so as to distinguish it from an ordinary force which can be balanced by a weight or a spring. Batra (1987) extended Eshelby's work to non-linear elastic materials by showing that the configurational force on a defect in such solids is also a true force exerted on the core of the defect by the surrounding medium. The formulation was given in terms of the inverse deformation gradient and results compared with Eshelby (1980)'s work on force on a disclination in a nematic liquid crystal.

For linear materials, the Peach-Koehler force as given by Eshelby (1951) is,

$$F_l = -\int_{\Gamma_c} \left[\frac{1}{2}\sigma_{ij}\epsilon_{ij}\delta_{kl} - \sigma_{ik}u_{i,l}\right] n_k \ \mathrm{d}\Gamma \tag{2.41}$$

where with reference to fig. 2.10, Γ_c is a closed contour around the dislocation and n is the unit outward normal of Γ_c. Rice (1968) showed that the integral in eq. 2.41 has the same values for all paths around a class of notches in two-dimensional deformation fields of linear or non-linear elastic materials. This integral is now widely known as Rice's path independent J-integral.

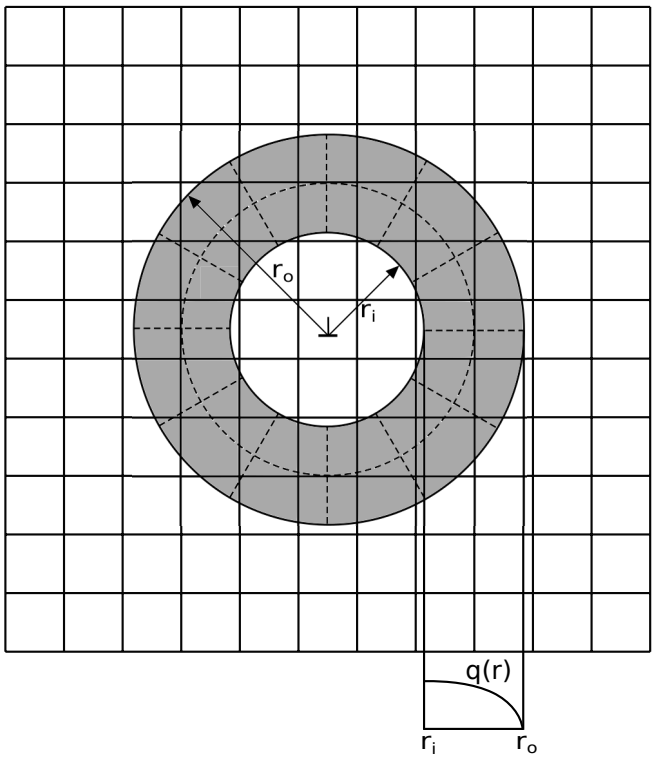

Figure 2.11: Structured integration domain for estimating the forces acting on the dislocation. The variation of the weight function $q(r)$ is also shown.

The contour integral discussed above is in a form that is ill-suited for finite element calculations as the stress fields of the finite element models are not continuous. For numerical purposes, it is beneficial to recast an area/domain form of the integral in lieu of the line/contour integral. Moran and Shih (1987) provided the domain form of the J-integral which is more accurate than the contour form. Using appropriate balance laws, crack tip flux integrals were derived and examined for path-independence in the crack-tip region to yield non-trivial results. The domain form of the J-integral is,

$$F_l = -\int_{\Omega_c} \left[\frac{1}{2}\sigma_{ij}\epsilon_{ij}\delta_{kl} - \sigma_{ik}u_{i,l} \right] q_{l,k} \ \mathrm{d}\Omega \tag{2.42}$$

where Ω_c is the domain containing the dislocation core bounded by Γ_c and q is the weight function. For the two-dimensional examples considered in this study, the energy released by a virtual advance of the dislocation is integrated over an area surrounding the dislocation. The integral in eq. 2.42 is numerically evaluated over

an annular region defined by $r_i < r < r_0$, around the dislocation. A local polar coordinate system is defined for the dislocation in terms of the level set functions. The coordinates of a point $x(\mathbf{r}, \theta)$ are associated with the global coordinates by,

$$\begin{aligned} x(\mathbf{r}, \theta) &= x_0 + rR\vec{\xi} \\ x_{\mathbf{I}} &= x_0 + r \begin{bmatrix} cos(\theta) & sin(\theta) \\ -sin(\theta) & cos(\theta) \end{bmatrix} \vec{\xi} \end{aligned} \tag{2.43}$$

where x_0 is the location of the dislocation. The domain form of the J-integral in polar coordinates will then be,

$$F_l = -\int_{r_i}^{r_0} \int_0^{2\pi} \left[\frac{1}{2}\sigma_{ij}\epsilon_{ij}\delta_{kl} - \sigma_{ik}u_{i,l} \right] q_{l,k} \ r\mathrm{d}r\mathrm{d}\theta \tag{2.44}$$

The vector field q as defined by Oswald *et al.* (2011) is chosen to be,

$$\begin{aligned} q(\mathbf{r}) &= \nabla g(\mathbf{x_0})\rho(\mathbf{r}) \\ \rho(\mathbf{r}) &= \frac{(r - r_0)^2}{(r_i - r_0)^2} \end{aligned} \tag{2.45}$$

One other possible way to integrate the integral in eq. 2.42 is by defining Ω_c to be a square with a thickness of $(r_o - r_i)$, centred at the dislocation core. The weight function q is defined to be equal to 1 at all nodes at a distance of r_i from the core and decreases linearly to 0 at r_o. The definition of Ω_c described above is based on that used by Dolbow and Belytschko (1999) for crack tips and is illustrated in fig. 2.12.

The domain Ω_c must contain only one dislocation core compelling the radius of the integral contour to be as small as possible in order to be able to implement the proposed XFEM method to dislocations. The domain form of the integral in eq. 2.42 contains the term, dq/dx which means that the integral will be evaluated only when $dq/dx \neq 0$. The integral is effectively evaluated around a contour surrounding the point of singularity. In the case when the dislocation is close to the boundary of the body, the area over which the integral is evaluated may not completely lie inside the

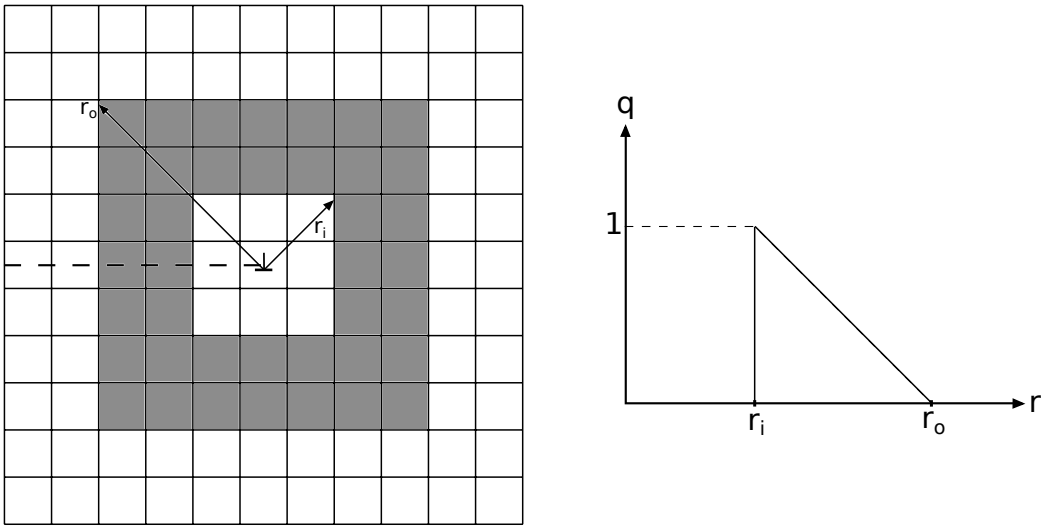

Figure 2.12: Left, Integration domain definition for the domain form of J-integral around a dislocation core. The weight function q has a value of 1 at a distance of r_i from the core and a value of 0 in the region outside of a distance of r_o from the core. Right, Weight function q as a function of distance r from the dislocation core.

body. Consequently, the integral would be evaluated along a contour not surrounding the point of singularity, resulting in the inaccurate representation of the dislocation energies involved.

Integrating the Element Containing the Dislocation Core

The integrand in eq. 2.16 and eq. 2.38 is discontinuous in the element containing the dislocation core as the Heaviside function of $g(\mathbf{x})$ in eq. 2.16 turns off in the element. The use of a few gauss quadrature points to integrate such a discontinuous function would introduce an error in the approximated displacement values. The accuracy at the dislocation core can be improved in one of the following three ways.

The parent element of the element containing the dislocation core can be divided into a large number of smaller squares and one integration point could be placed at the centre of every square with equal weights being assigned to every integration point. Although expensive, the need to do this for only one element justifies its use to improve the accuracy of integration at the core.

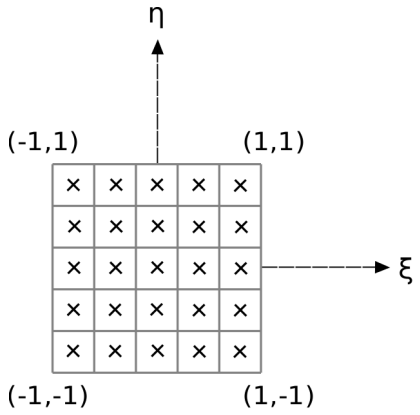

Figure 2.13: The parent element is divided into smaller squares with an integration point at the centre of each square. Equal weights are assigned to each integration point.

Another possible method to improve the accuracy of integration would involve shifting the dislocation to an element edge in the pre-processing stage as seen in fig. 2.14. In doing so, the integrand would no longer be discontinuous in the element containing the dislocation as $H(g(\mathbf{x}))$ would turn off only at the element edge, ensuring that the entire core element has been integrated. Once the element containing the dislocation is identified, the points at which the glide plane $f(\mathbf{x}) = 0$, intersects the element edges are determined. The distance of these points from the dislocation $g(\mathbf{x})$, is calculated using parts of algorithm 2 and the dislocation is moved along the glide plane to the nearest intersection point. The distance of the dislocation from the free surface is accordingly updated.

Yet another method that can be used to evaluate the integrand precisely in the element containing the dislocation consists of dividing said element into smaller areas for integration. The region of the core element in which $H(g(\mathbf{x}))$ is active is split into smaller areas and these smaller areas are then individually integrated using integration points defined by gauss quadrature. Evaluating the integrand in the region of the core element in which $H(g(\mathbf{x}))$ is inactive is not necessary as the enrichment function has been turned off in that region of the core element. In the example illustrated by

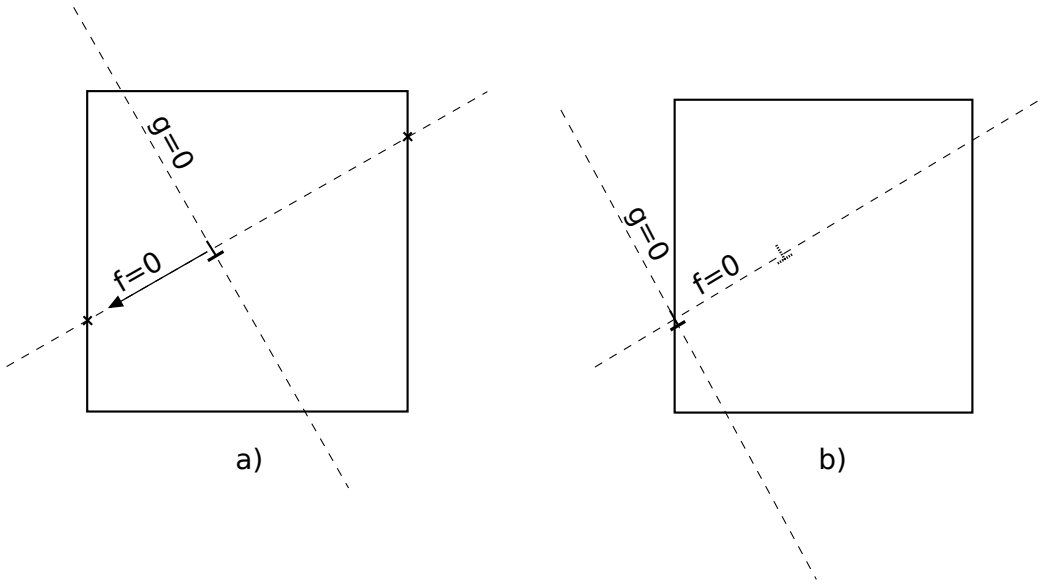

Figure 2.14: Illustration of shifting the dislocation to an element edge. a) The element containing the dislocation is identified and points at which the glide plane intersects the element edges are marked b) The dislocation is shifted to the nearest edge

fig. 2.15, the core element has been divided into triangles by considering the points at which $g(\mathbf{x}) = 0$ intersects the element edges, the location of the dislocation and nodal positions. These triangles in their natural coordinates are then transformed into quadrilaterals by repeating a local nodal position. The integrand is now evaluated at the integration points in the transformed element and combined with similar results from the other triangles.

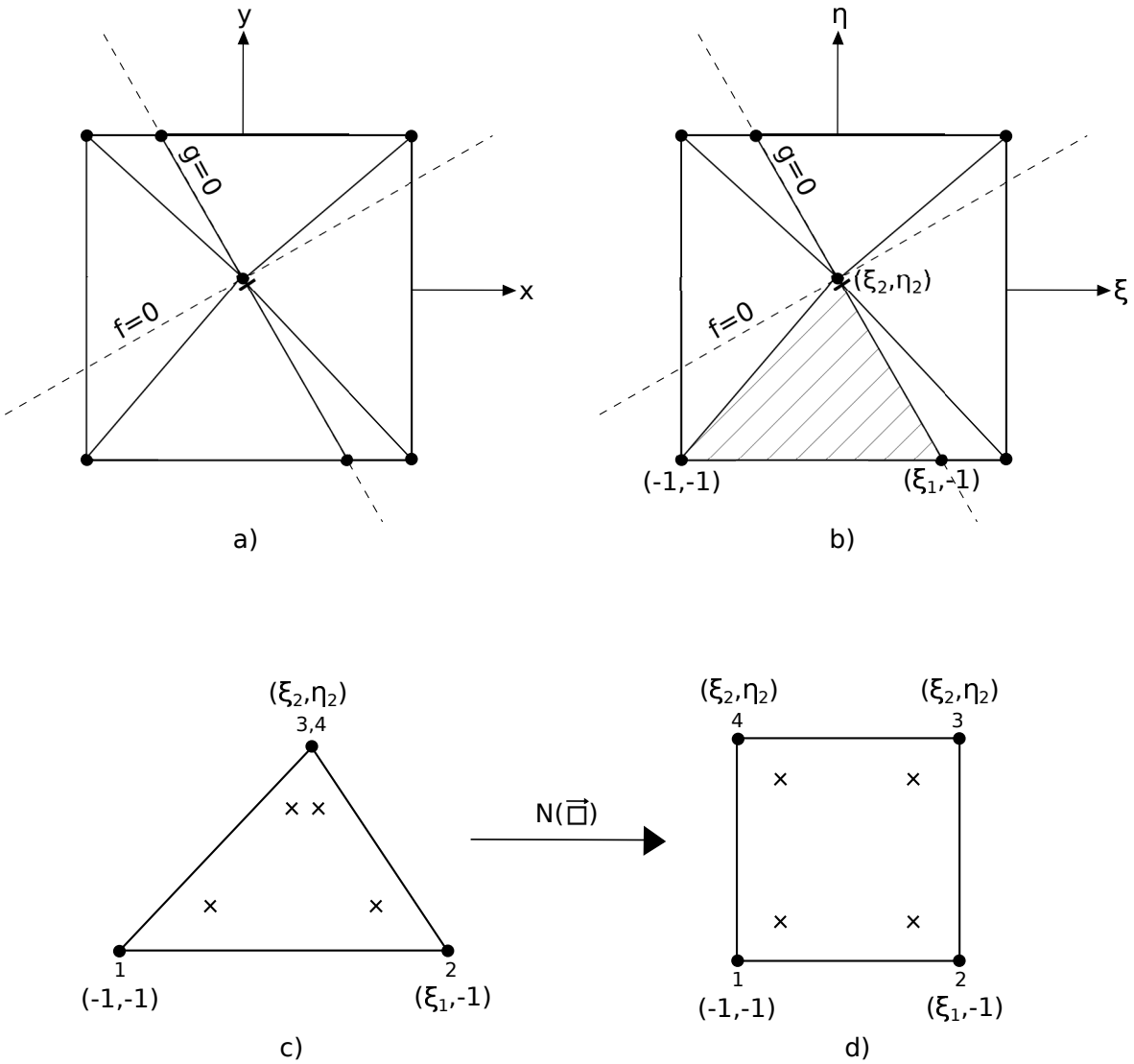

Figure 2.15: Illustration of dividing the core element into triangles for improving the accuracy of integration. a) Core element is divided into triangles by identifying the nodal positions, dislocation location and points where $g(\mathbf{x}) = 0$ intersects the element edges b) depicts the local coordinates of the triangular element under consideration c) Integration points defined by gauss quadrature are placed in the triangle d) shows the triangular element transformed into a quadrilateral element

Chapter 3

RESULTS AND ANALYSIS

3.1 Dislocation in a Semi-infinite Domain

To simulate an edge dislocation in a semi-infinite domain near a free surface, a 1×1 µm domain containing a dislocation core with a horizontal glide plane as shown in fig. 3.1 is considered. The free surface is located at $x = 0$ and the domain is then defined by $-L < x < L$ and $-L < y < L$. The dislocation is located at a distance of $L = 0.5$ µm from the free surface and the glide plane is perpendicular to the free surface, along $y = 0$. The elastic modulus, Poisson's ratio and the magnitude of Burgers vector are 121.41×10^3 MPa, 0.34 and 8.551×10^{-4} µm respectively. A structured and an unstructured mesh of four-noded quadrilateral elements as shown in fig. 3.2 are used. Along the top, bottom and right boundaries of the domain, a displacement boundary condition corresponding to the analytical solution for an edge dislocation near a free surface, as given by Head (1953a) in eq. 3.1 and eq. 3.2, is applied.

$$
\begin{aligned}
\sigma_{xx} &= \frac{Eb}{4\pi(1-\nu^2)}\left[-\frac{y\left(3(x-L)^2+y^2\right)}{\left((x-L)^2+y^2\right)^2}+\frac{y\left(3(L+x)^2+y^2\right)}{\left((L+x)^2+y^2\right)^2}\frac{4Lxy\left(3(L+x)^2-y^2\right)}{\left((L+x)^2+y^2\right)\left((L+x)^2+y^2\right)}\right]\\
\sigma_{yy} &= \frac{Eb}{4\pi\left(1-\nu^2\right)}\left[\frac{y\left((x-L)^2-y^2\right)}{\left((x-L)^2+y^2\right)^2}-\frac{y\left((L+x)^2-y^2\right)}{\left((L+x)^2+y^2\right)^2}+\frac{4Ly\left(y^2(2L+3x)+(2L-x)(L+x)^2\right)}{\left((L+x)^2+y^2\right)^3}\right]\\
\sigma_{xy} &= \frac{Eb}{4\pi\left(1-\nu^2\right)}\left[\frac{(x-L)\left((x-L)^2-y^2\right)}{\left((x-L)^2+y^2\right)^2}-\frac{(L+x)\left((L+x)^2-y^2\right)}{\left((L+x)^2+y^2\right)^2}+\frac{2L\left(6xy^2(L+x)+(L-x)(L+x)^3-y^4\right)}{\left((L+x)^2+y^2\right)^3}\right]
\end{aligned}
\tag{3.1}
$$

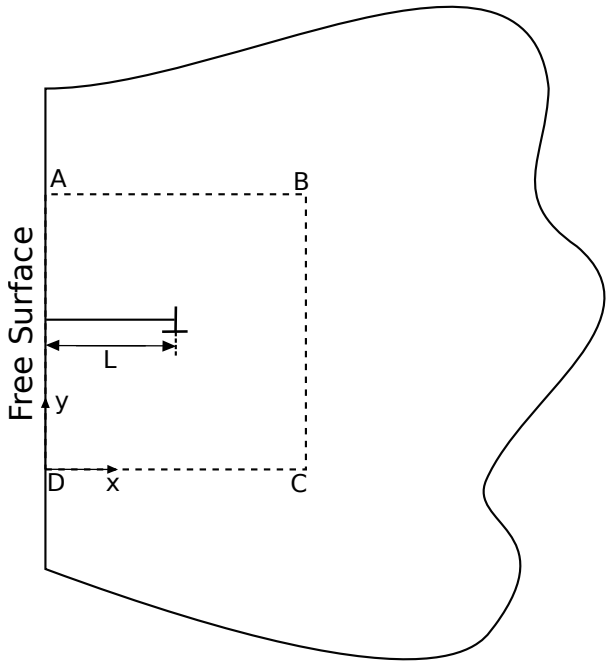

Figure 3.1: An edge dislocation in a semi-infinite domain, close to a free surface. The subdomain ABCD is the numerical simulation domain.

$$
\begin{aligned}
u_x = \frac{by}{4\pi(\nu-1)}\Bigg[&\frac{-4L\nu+7L+x}{L^2+2Lx+x^2+y^2}+\frac{L-x}{L^2-2Lx+x^2+y^2}-\frac{4L\left(L^2+Lx+y^2\right)}{\left(L^2+2Lx+x^2+y^2\right)^2}\\
&+\frac{2(\nu-1)\tan^{-1}\left(\frac{L-x}{y}\right)}{y}+\frac{2(\nu-1)\tan^{-1}\left(\frac{L+x}{y}\right)}{y}\Bigg]\\
u_y = \frac{b}{8\pi(\nu-1)}\Bigg[&-\frac{2\left(L^2(4\nu-3)+4L(\nu-1)x+x^2\right)}{L^2+2Lx+x^2+y^2}+(1-2\nu)\log\left(L^2-2Lx+x^2+y^2\right)\\
&+(2\nu-1)\log\left(L^2+2Lx+x^2+y^2\right)+\frac{2(L-x)^2}{L^2-2Lx+x^2+y^2}-\frac{8Lx(L+x)^2}{\left(L^2+2Lx+x^2+y^2\right)^2}\Bigg]
\end{aligned}
\tag{3.2}
$$

The shear stress along the glide plane, $f(\mathbf{x}) = 0$ is plotted in fig. 3.8 against the exact solution. It is evident that the shear stress is captured perfectly away from the dislocation core. The stress near the core is only approximately captured as the enrichment approximation, eq. 2.16 is a regularization of the step discontinuity of the exact solution. The regularization of the step discontinuity approaches a step discontinuity with mesh refinement leading the shear stress near the core to be accurate.

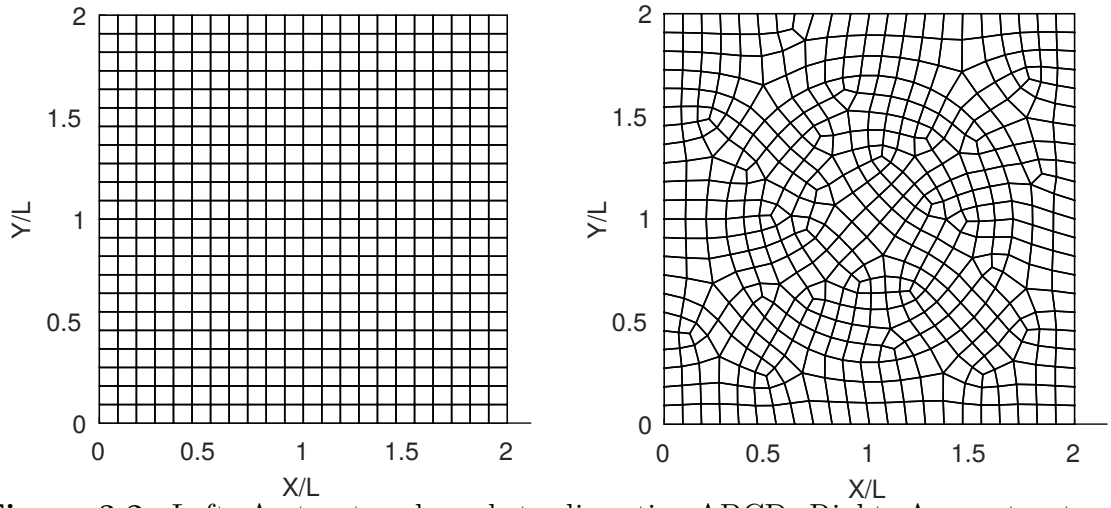

Figure 3.2: Left, A structured mesh to discretize ABCD. Right, An unstructured mesh to discretize ABCD

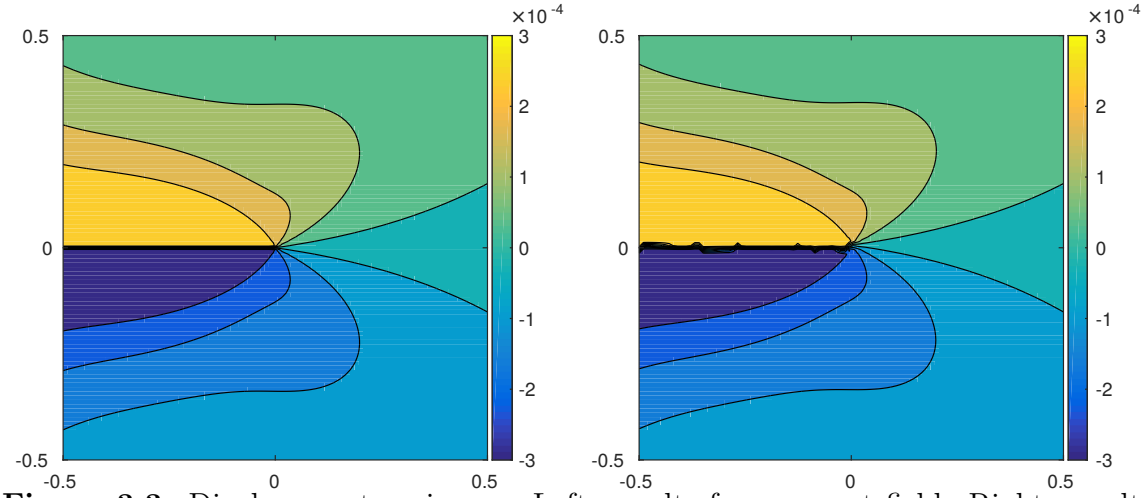

Figure 3.3: Displacement u_x in µm. Left, results for an exact field. Right, results using XFEM for an unstructured mesh

Figures 3.3 - 3.7 show that the proposed method correctly estimates the displacement and stress fields for a dislocation near a free surface.

In order to study the accuracy of the Peach-Koehler force estimated by the domain form of J-integral in eq. 2.42, the domain of integration, Ω_c is fixed. An annular shaped domain with $r_i/L = 0.2$ and $r_o/L = 0.4$ around the dislocation core is chosen as per fig. 2.11. The domain over which the J-integral was evaluated was chosen to be larger than would be in an actual simulation in order to accommodate coarser meshes in the

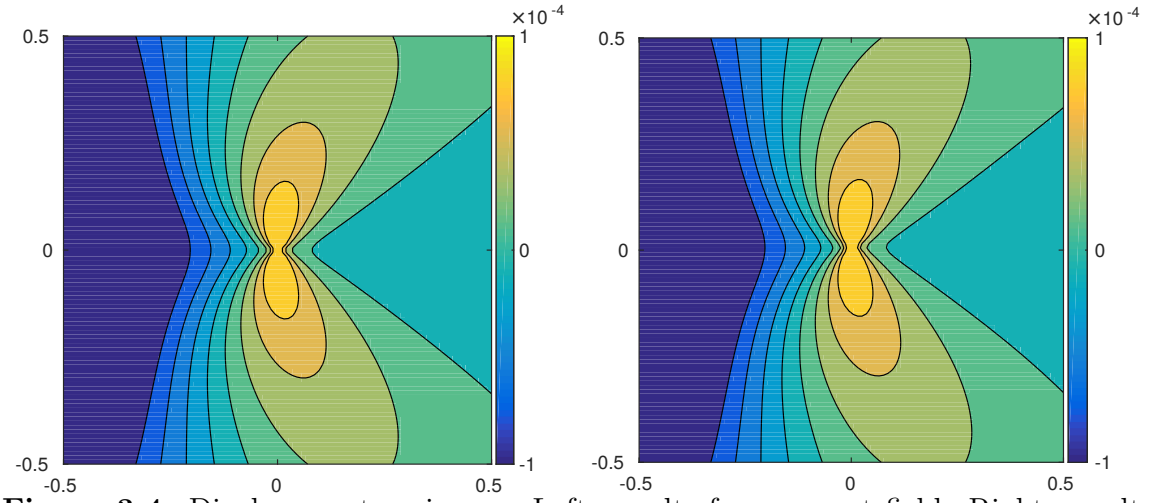

Figure 3.4: Displacement u_y in µm. Left, results for an exact field. Right, results using XFEM for an unstructured mesh

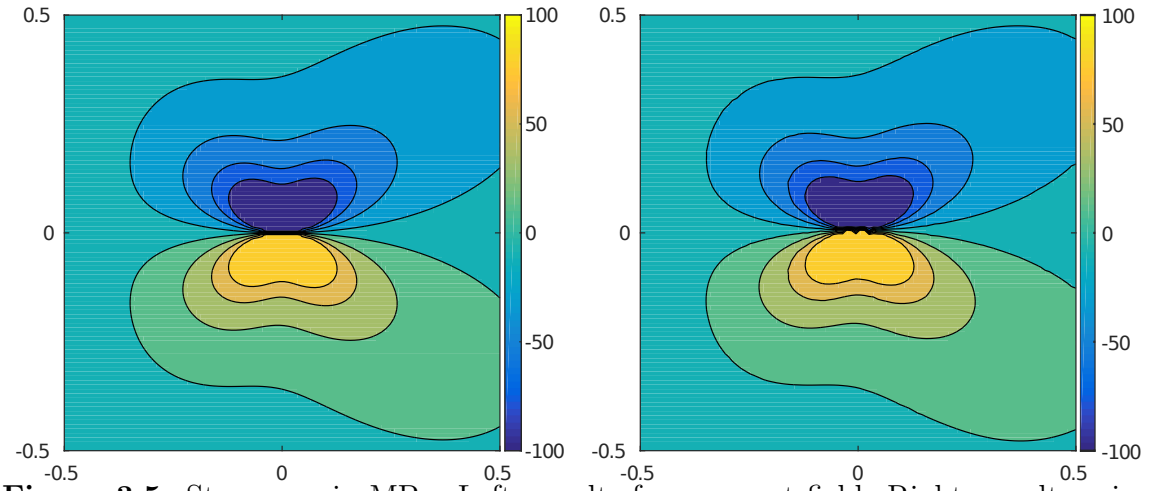

Figure 3.5: Stress σ_{xx} in MPa. Left, results for an exact field. Right, results using XFEM for an unstructured mesh

convergence study. Fig. 3.10 and fig. 3.11 show the convergence of the relative error in computing the Peach-Koehler force in the glide direction with decreasing element size for a structured mesh and an unstructured mesh respectively. The relative error converges at a rate of 2.0 with respect to the element size in both cases. Thus the proposed method approximates the glide force well and the glide force converges to the exact solution at an optimal rate of h_e^2 for linear finite elements over a fixed area around the core; h_e is the element size.

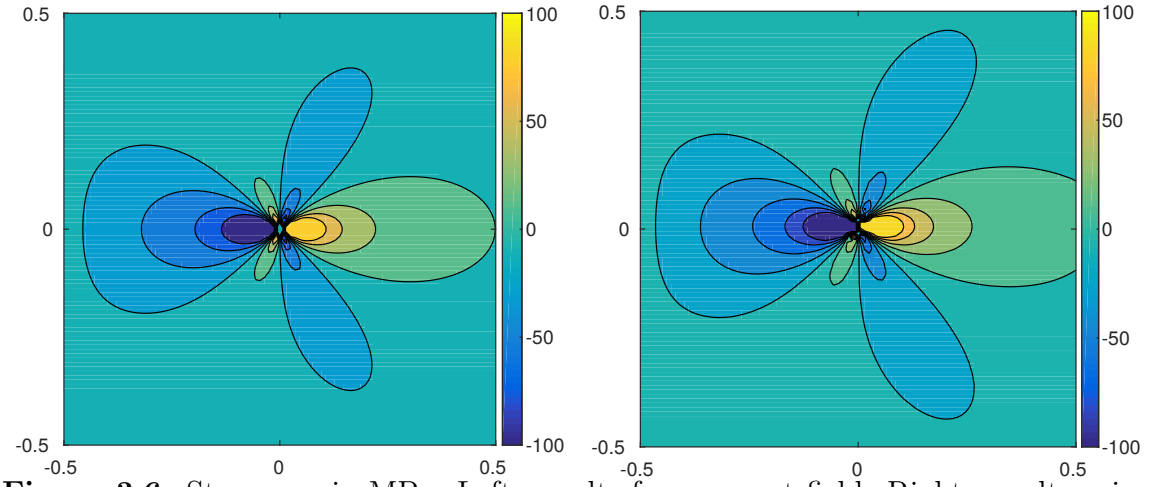

Figure 3.6: Stress σ_{xy} in MPa. Left, results for an exact field. Right, results using XFEM for an unstructured mesh

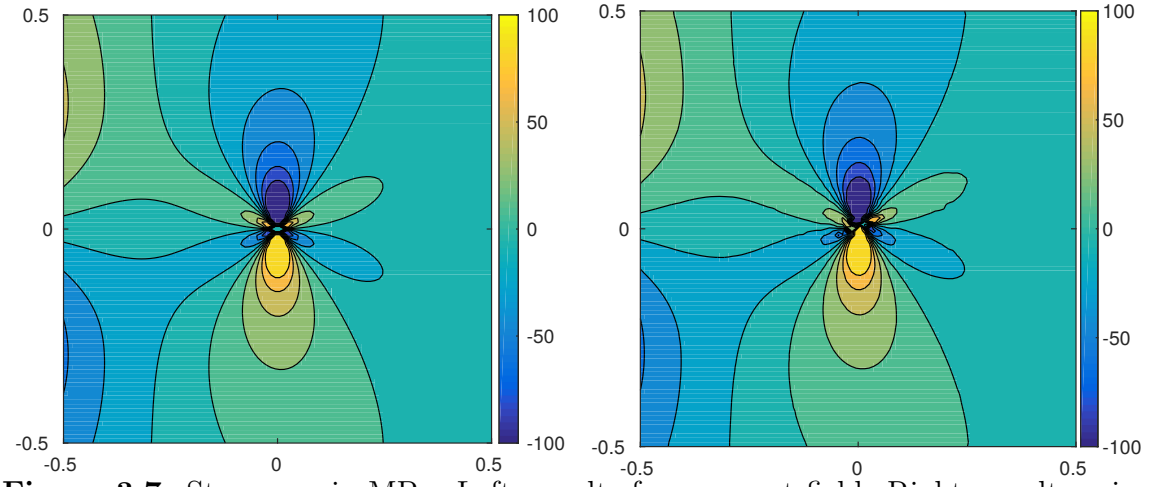

Figure 3.7: Stress σ_{yy} in MPa. Left, results for an exact field. Right, results using XFEM for an unstructured mesh

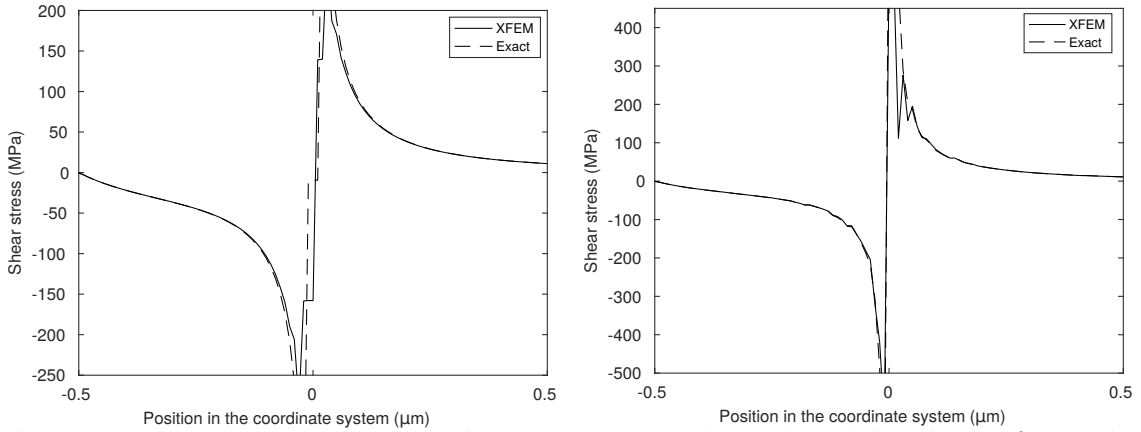

Figure 3.8: XFEM and exact shear stress σ_{xy} along the glide plane of an edge dislocation near a free surface for a structured mesh on the left and for an unstructured mesh on the right; $h_e \approx 10\,\text{nm}$. The dislocation core is located at $x = 0$.

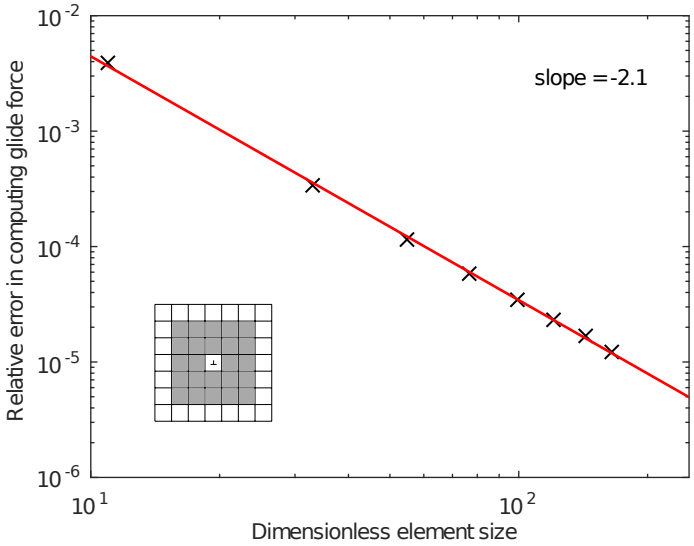

Figure 3.9: Convergence of the Peach-Koehler force for a structured mesh. The integration domain definition used in fig. 2.12 was employed.

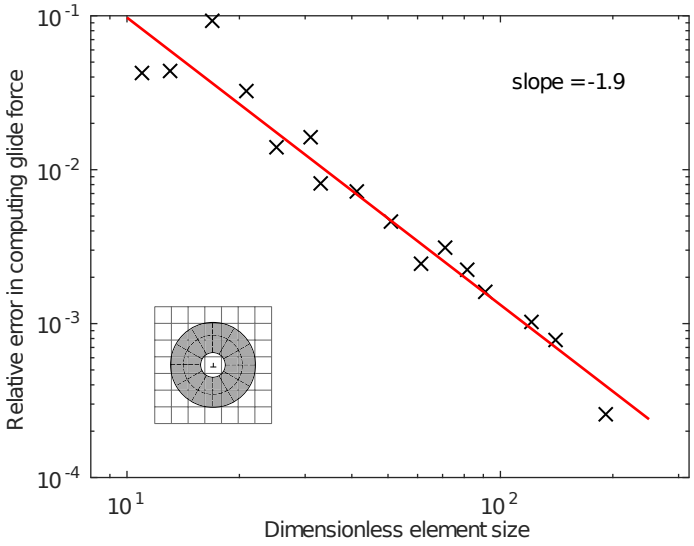

Figure 3.10: Convergence of the Peach-Koehler force for a structured mesh. The integration domain definition used in fig. 2.11 was employed.

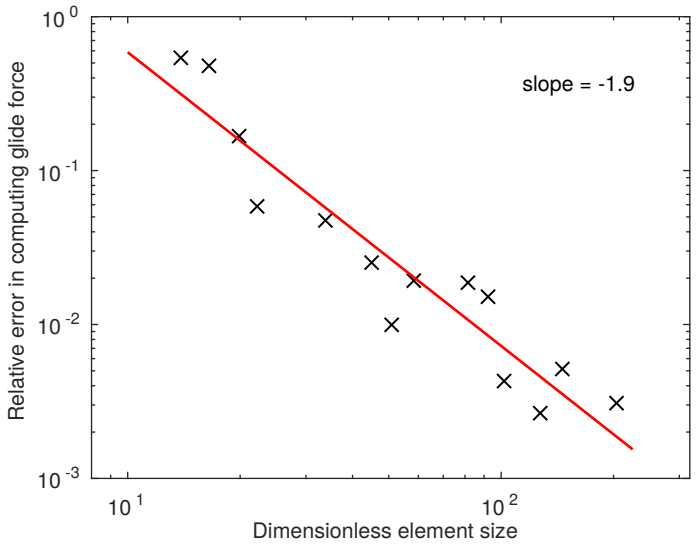

Figure 3.11: Convergence of the Peach-Koehler force for an unstructured mesh. The integration domain definition used in fig. 2.11 was employed.

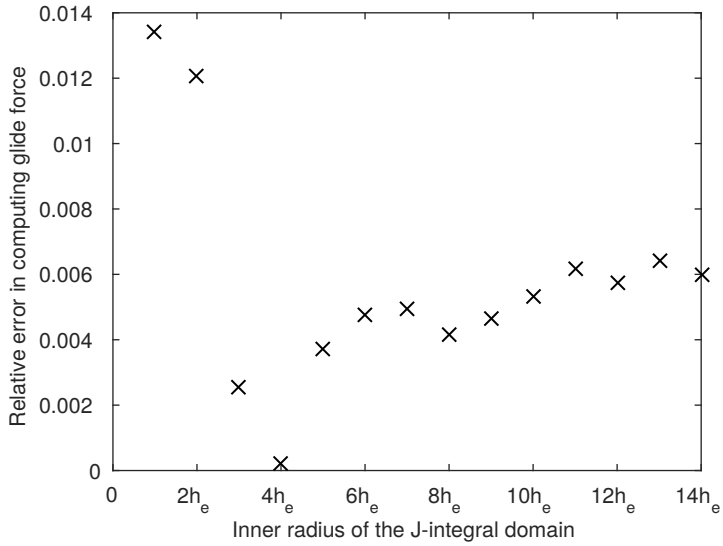

Figure 3.12: Peach-Koehler force for various inner radius of the integration domain for an unstructured mesh of about 100×100 elements; $h_e \approx 10\,\text{nm}$.

In studying the convergence of the Peach-Koehler force for a structured mesh, a square shaped domain with $r_i/L = 0.3$ and $r_o/L = 0.7$ around the dislocation was also chosen as per fig. 2.12. The relative error converges at a rate of about 2.0 with respect to the element size as well. This domain definition performed poorly for an unstructured mesh and was hence not included in this study.

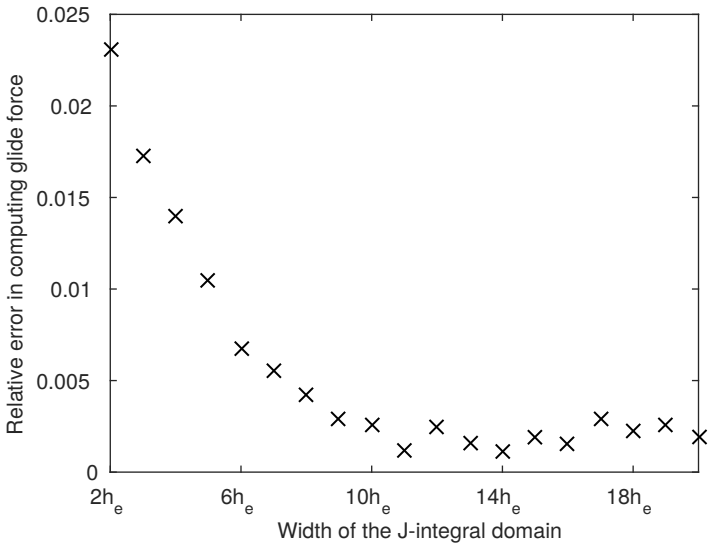

Figure 3.13: Peach-Koehler force for various width (thickness) of the integration domain for an unstructured mesh of about 100×100 elements; $h_e \approx 10\,\text{nm}$.

Integration domains of different sizes were also considered for an unstructured mesh of about 100×100 elements, with an approximate element size of 10 nm. Fig. 3.12 illustrates the relative error in computing the Peach-Koehler force for various values of the inner radius of the integration domain. The inner radius is considered in terms of the number of elements away from the dislocation core. From the figure, it is evident that when the inner radius is relatively small, increasing it improves the accuracy of J-integral. This shows that the stress field at the core is not accurately captured and that it is less accurate close to the core than slightly farther away from the core. But, beyond a certain point in the domain, increasing the inner radius reduces the accuracy by a small amount. Hence, the inner radius of the integration domain must be selected sufficiently far from the core but yet in the vicinity of the core. Fig. 3.13 illustrates the Peach-Koehler force and the relative error for various values of thickness (width) of the integration domain. The thickness is also considered in terms of the number of elements across the integration domain in an average sense. The figure depicts that the accuracy of J-integral is poor for too thin an integration domain.

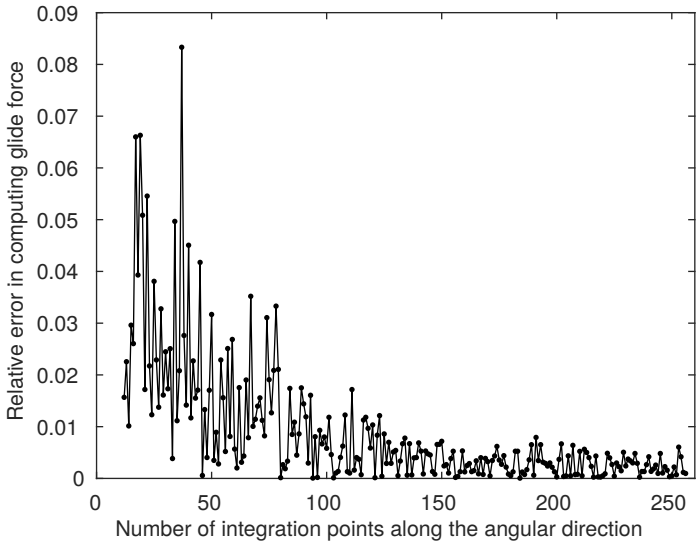

Figure 3.14: Variation of the Peach-Koehler force with the number of integration points chosen in the angular direction for an unstructured mesh of about 100×100 elements; $h_e \approx 10\,\text{nm}$.

The accuracy increases with increasing thickness but only to a certain point, beyond which increasing the domain thickness has no effect on the accuracy.

Fig. 3.14 shows the variation in the relative error in computing the Peach-Koehler force for an increasing number of integration points in the angular direction. The integration points were distributed in the angular direction using the trapezoidal rule. The error reduces with increasing number of integration points until a certain range of values beyond which the error remains nearly unchanged. Fig. 3.15 depicts the variation in the relative error in computing the Peach-Koehler force for an increasing number of integration points in the radial direction. The integration points were spread in the radial direction using gauss quadrature. The error also reduces with increasing number of integration points but a very large number of integration points would only be fitting a polynomial through the noise that may have been captured in the integration domain. Thus the number of integration points in the radial and angular direction must be chosen sufficiently large enough but yet not large enough to cause overfitting and lead to longer computation time.

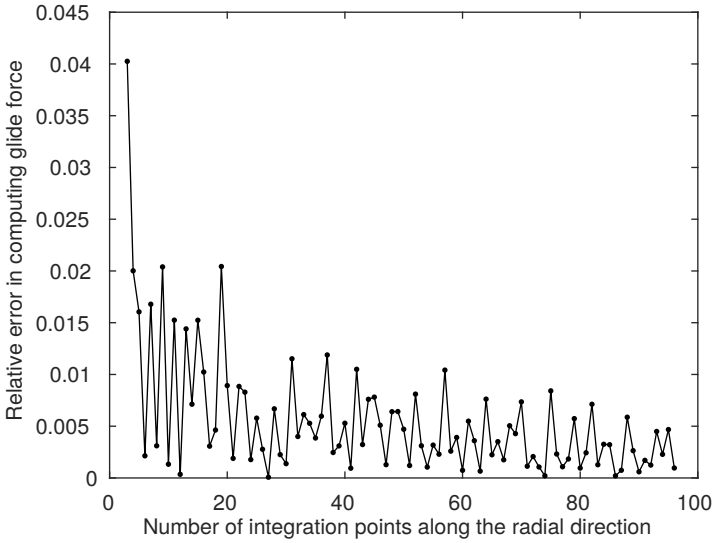

Figure 3.15: Variation of the Peach-Koehler force with the number of integration points chosen in the radial direction for an unstructured mesh of about 100×100 elements; $h_e \approx 10\,\text{nm}$.

3.2 Dislocation near a Single Inclusion

Aluminium-copper (Al-Cu) alloy films are extensively used for interconnects in integrated circuits. Ames *et al.* (1970) found that the lifetime of aluminium films subjected to high current densities at elevated temperatures could be improved by adding copper to the films. This discovery resulted in extensive examination of Al-Cu thin films and lines. The amount of copper added usually varies from 0.2% to 2%. At temperatures above 500°C, copper remains suspended in the solid solution but at room temperatures, most copper will be incorporated into the matrix as Al_2Cu precipitates. Gardner and Flinn (1990) reported volume changes during the solid solution-precipitate transformation to be a source of localised stress fields. Other phenomena that contribute to stress changes include elastic behaviour (mismatch), recrystallization, grain growth, plastic behaviour, yield strength, and film hardening from precipitates. Material properties such as yield strength, ductility, etc. of the matrix are affected by the presence of these precipitates. Therefore, the interaction

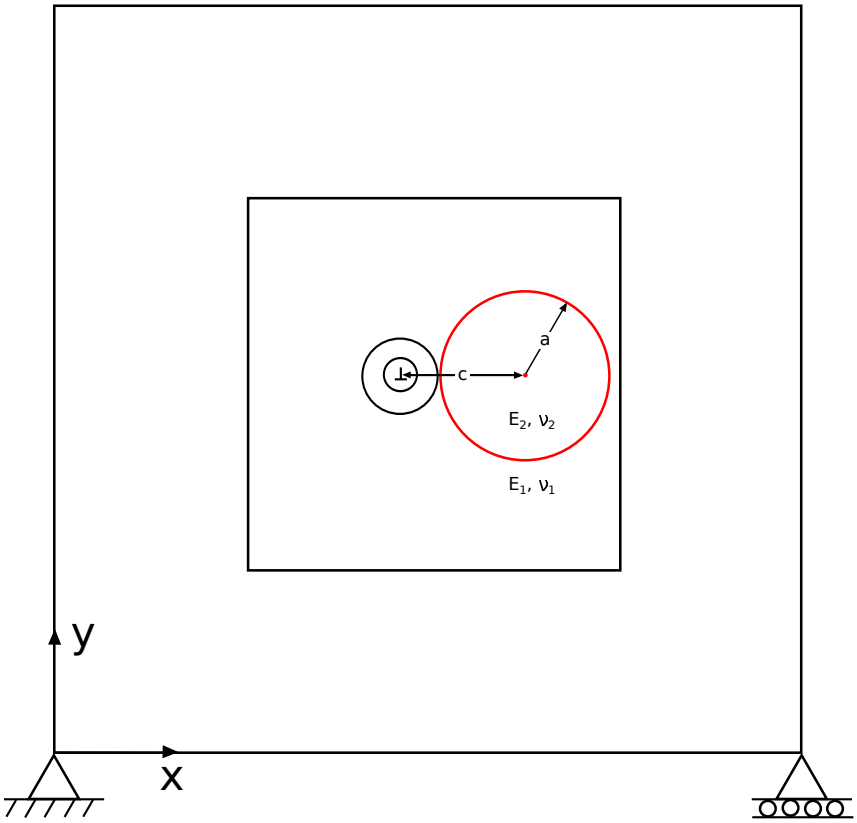

Figure 3.16: Nomenclature for an edge dislocation interaction with a circular inclusion.

between an edge dislocation and these precipitates is considered in this section.

To simulate the above scenario, an edge dislocation near a circular inclusion in a 1×1 µm domain as shown in fig. 3.16 is considered. The domain is supported so as to prevent rigid body motion. The domain is discretized into an unstructured mesh of four-node quadrilateral elements. A circular inclusion of radius $a = 0.15$ µm is located with its centre on the glide plane $f(\mathbf{x}) = 0$, of the dislocation with a Burgers vector of 8.551×10^{-4} µm. The Aluminium matrix has an elastic modulus of $E_1 = 70 \times 10^3$ MPa and a Poisson's ratio of $\nu_1 = 0.345$ and the Al_2Cu precipitate has an elastic modulus of $E_2 = 99 \times 10^3$ MPa and a Poisson's ratio of $\nu_2 = 0.345$. The solution to this problem was given by Head (1953b) and later used to study the Peach-Koehler force on an edge dislocation near a circular inclusion by Dundurs and Mura (1964).

They calculated the force on the dislocation to be,

$$F = -\frac{G_1 b^2}{\pi(\kappa_1 + 1)a} \ \frac{1}{\beta} \left(\frac{B + A}{\beta^2 - 1} + \frac{3A - B}{\beta^2} \right) \tag{3.3}$$

Herein,

$$\beta = \frac{c}{a} \geq 1 \tag{3.4}$$

and

$$A = \frac{1 - \Gamma}{1 + \Gamma\kappa_1}, \qquad B = \frac{\kappa_2 - \Gamma\kappa_1}{\kappa_2 + \Gamma} \tag{3.5}$$

where

$$\Gamma = \frac{G_2}{G_1} \tag{3.6}$$

where G is the shear modulus, $\kappa = 3 - 4\nu$ for plane strain and $\kappa = 3 - 4\nu$ for plane stress, ν being the Poisson's ratio. a is the radius of the inclusion, c is the distance of the dislocation from the centre of the inclusion, b is the Burgers vector of the dislocation, and '1' and '2' refer to the matrix and the inclusion respectively.

In order to eliminate the effect of free surfaces on the computational results, the domain under consideration is embedded at the centre of a much larger domain; the 1×1 µm domain is placed at the centre of a 10×10 µm domain. The larger domain is discretized to have a coarse mesh that linearly refines into a finer mesh in the computational domain under consideration as shown in fig. 3.17 .

The glide component of the Peach-Koehler force obtained by using XFEM is compared to that from eq. 3.3 for various distances between the dislocation and the circular inclusion in fig. 3.18. It is evident from the plot that the force experienced by the dislocation increases as it approaches the inclusion. The force being repulsive is due to the larger elastic modulus of the inclusion than the matrix containing the dislocation. When the elastic modulus of the matrix is larger than that of the inclusion, the dislocation will be attracted to the inclusion as it moves in the vicinity of the inclusion. This force of attraction increases as the dislocation approaches

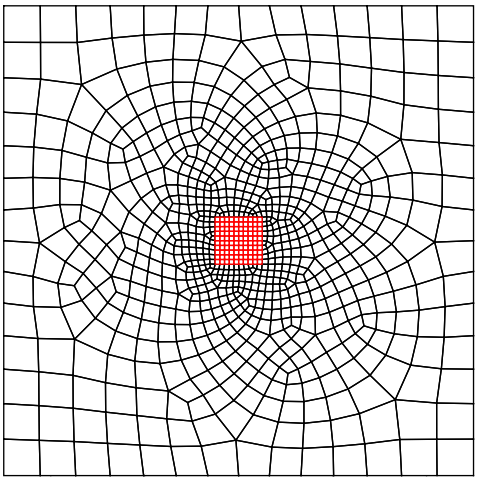

Figure 3.17: The computational domain (in red) is embedded in a much larger domain to eliminate the influence of the free surfaces.

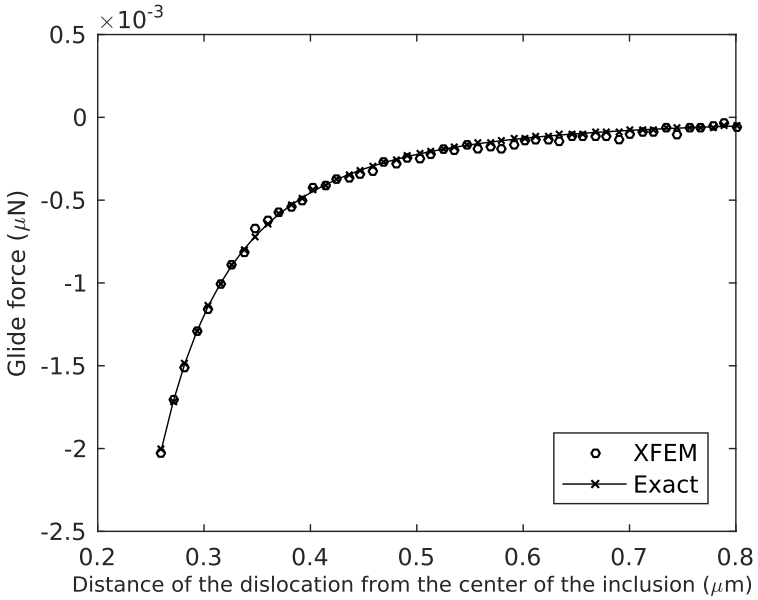

Figure 3.18: Comparison of the glide component of the Peach-Koehler force calculated using XFEM with the exact result for an edge dislocation near a circular inclusion.

the inclusion as well. As can be seen, the Peach-Koehler force computed using the domain form of J-integral with $r_i = 4h_e$ and $r_o = 8h_e$ compares well with the exact solution. The accuracy reduces due to inadequate mesh resolution as the dislocation approaches the inclusion. Mesh refinement near the inclusion can be used to increase the accuracy of the glide force estimation. This can easily be achieved as the element edges do not have to conform to the glide plane when using XFEM.

Precipitates in alloys or composites may occur in the shape of a cube depending on the shape of the constituents. An inclusion in the shape of a square with the equal area and similar material properties as the aforementioned circular inclusion is considered in the following analysis. The square shaped inclusion with an edge length of 0.265 µm is located with its centre on the glide plane. Two orientations of the square shaped inclusions are considered, one with its edges perpendicular to the glide plane (referred to as square shaped inclusion in this study) and the other with its diagonals perpendicular to the glide plane (referred to as diamond shaped inclusion in this study). Fig. 3.19 shows a comparison of the Peach-Koehler force for an edge dislocation approaching the centre of a circular, square shaped and diamond shaped inclusion. All the inclusions are located at the same point in the domain. The dislocation experiences greater repulsive force when approaching the diamond shaped inclusion as the elastic mismatch between a circular inclusion and the matrix is evenly distributed along the circumference of the circular inclusion whereas the elastic mismatch is concentrated at the sharp corners of a square and diamond shaped inclusion. Therefore, a dislocation approaching the corners of an inclusion with sharp corners will tend to experience a greater force than from any part of the circular inclusion.

The size of the inclusion also affects the force on the dislocation. When the radius of the circular inclusion and the edge length of the square and diamond shaped

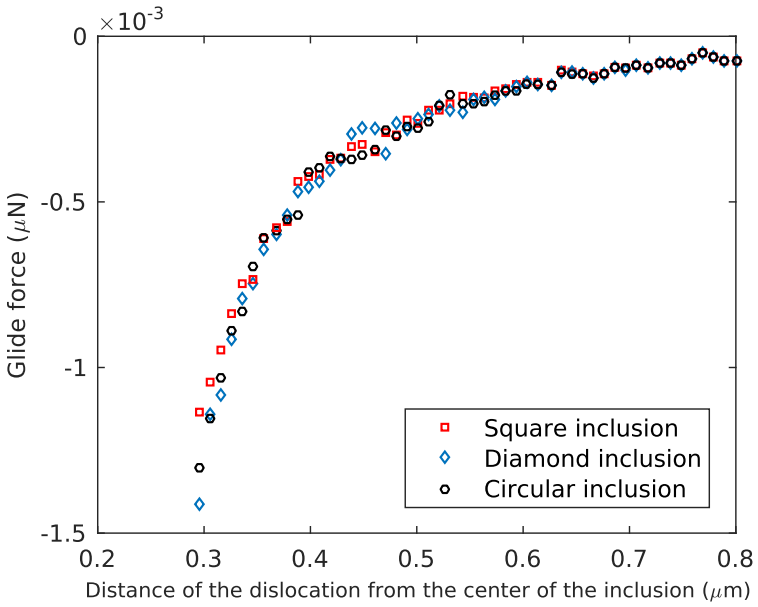

Figure 3.19: Comparison of the Peach-Koehler force for an edge dislocation near a circular, square shaped and diamond shaped inclusion.

inclusions were halved, with their centres at the same point, the glide force on the dislocation is as shown in fig. 3.20. It can be seen from the figures that force on the dislocation reduces as the size of the inclusion reduces. Again, the force due to the diamond shaped inclusion is slightly more than that from the circular inclusion.

In studies by Arsenault and Fisher (1983), Arsenault and Shi (1986) and Chawla and Metzger (1972), the difference in coefficient of thermal expansion between the inclusion and the matrix containing the inclusion was the source of high dislocation density generation at the inclusion-matrix interface. This thermal mismatch caused changes to the mechanical properties of the material. As the solid solution cools from processing temperatures of about 500°C to room temperature, Al_2Cu particles coalesce into precipitates that attract or repel dislocations in their vicinity based on their thermal and elastic mismatch with the aluminium matrix. Thermal stresses for a circular, square shaped and diamond shaped Al_2Cu particle in Al matrix is shown in fig. 3.21.

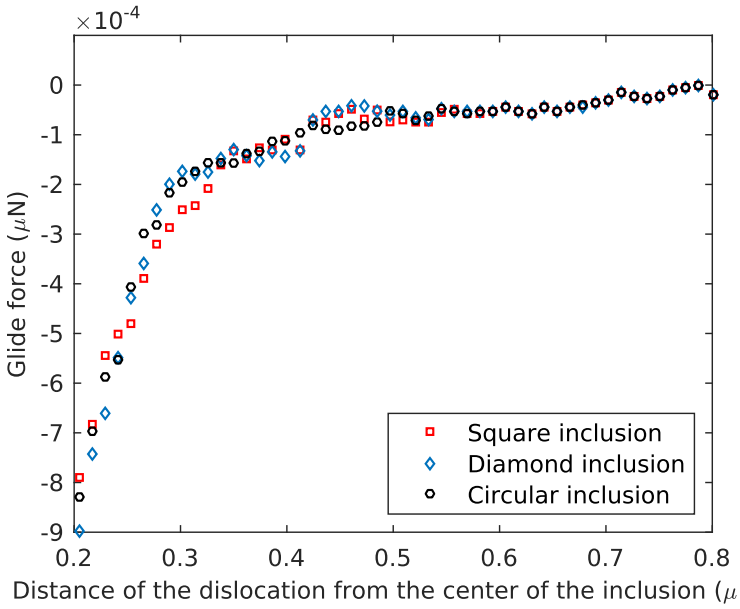

Figure 3.20: Comparison of the Peach-Koehler force for an edge dislocation near a smaller circular, square shaped and diamond shaped inclusion.

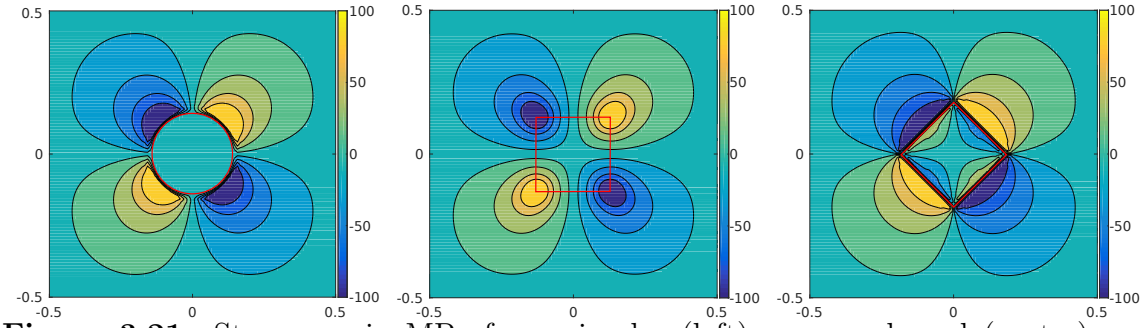

Figure 3.21: Stress σ_{xy} in MPa for a circular (left), square shaped (centre) and diamond shaped (right) Al_2Cu particle inside an Al matrix with elastic and thermal mismatch.

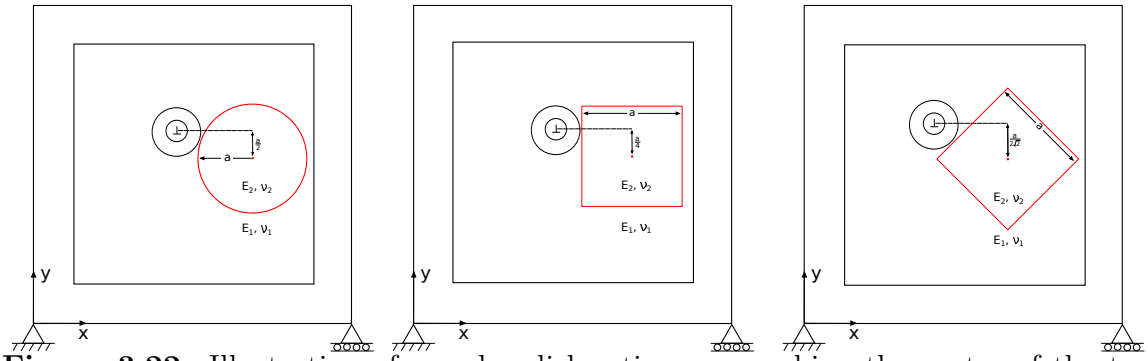

Figure 3.22: Illustration of an edge dislocation approaching the centre of the top half of a circular (left), square shaped (centre) and diamond shaped (right) Al_2Cu particle in an Al matrix with elastic and thermal mismatch.

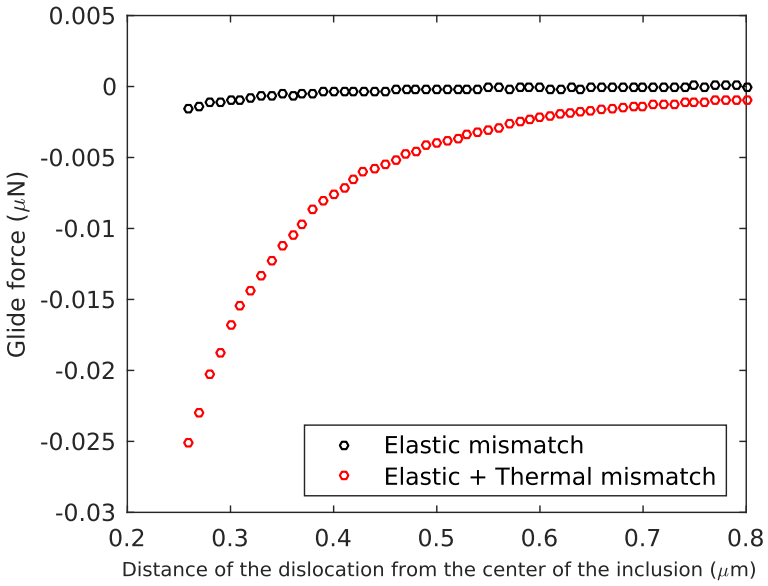

Figure 3.23: The Peach-Koehler force due to thermal mismatch for an edge dislocation approaching the centre of the top half of a circular inclusion.

Fig. 3.23 shows the Peach-Koehler force on the dislocation due to elastic mismatch and elastic as well as thermal mismatch in approaching the centre of the top half of the circular inclusion (see fig. 3.22). The dislocation is now repelled from the inclusion with a force augmented by the thermal mismatch between the aluminium matrix with a coefficient of thermal expansion of $24 \times 10^{-6}\mathrm{C}^{-1}$ and the Al_2Cu precipitate with a coefficient of thermal expansion of $16.2 \times 10^{-6}\mathrm{C}^{-1}$. Fig. 3.24 depicts the comparison of the Peach-Koehler force experienced by the dislocation due to thermal mismatch in approaching the centre of the top half of a circular, square and diamond shaped inclusion.

Fig. 3.26 depicts the comparison of the Peach-Koehler force experienced by the dislocation due to thermal mismatch in approaching the top of a circular, square and diamond shaped inclusion (see fig. 3.25).

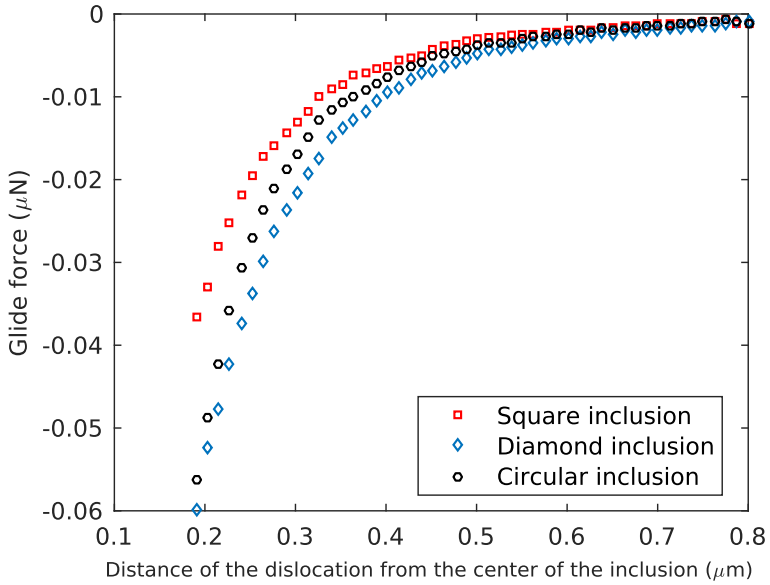

Figure 3.24: Comparison of the Peach-Koehler force due to thermal mismatch for an edge dislocation approaching the centre of the top half of a circular, square and diamond shaped inclusion.

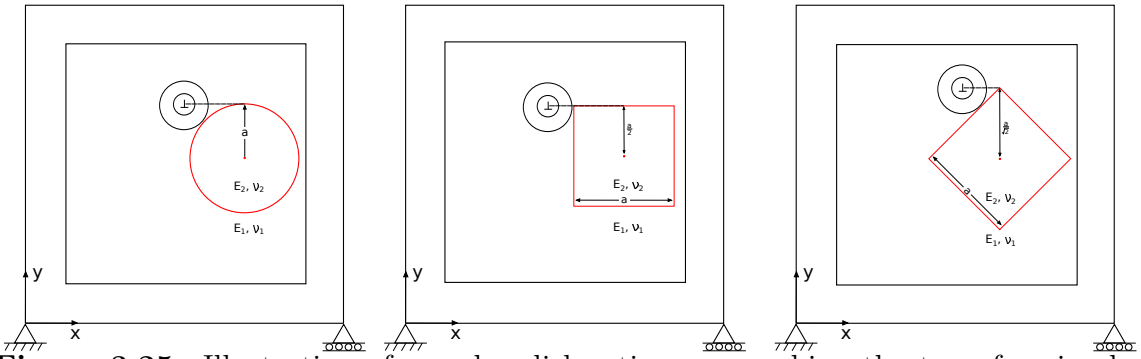

Figure 3.25: Illustration of an edge dislocation approaching the top of a circular (left), square shaped (centre) and diamond shaped (right) Al_2Cu particle in an Al matrix with elastic and thermal mismatch.

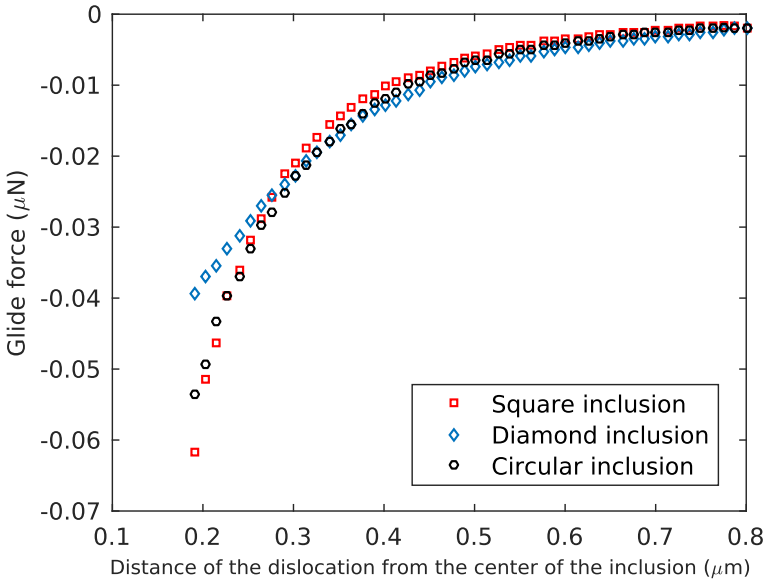

Figure 3.26: Comparison of the Peach-Koehler force due to thermal mismatch for an edge dislocation approaching the top of a circular, square and diamond shaped inclusion.

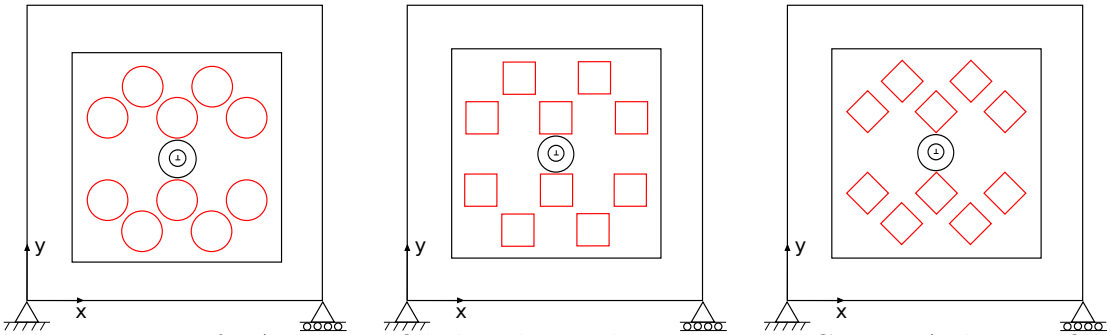

Figure 3.27: Left, A domain filled with circular inclusions. Centre, A domain filled with square shaped inclusions. Right, A domain filled with diamond shaped inclusions

3.3 Dislocation near Multiple Inclusions

A 1×1 µm domain with an array of circular inclusions is considered. This computational domain is embedded into a 10×10 µm domain in order to reduce the effect of free surfaces on the results as shown in fig. 3.17. The domain is supported so as to prevent rigid body motion. The Peach-Koehler force due to elastic mismatch on an edge dislocation with a Burgers vector of 8.551×10^{-4} µm, as it travels in an Al matrix filled with circular Al_2Cu precipitates is shown in fig. 3.28. As the

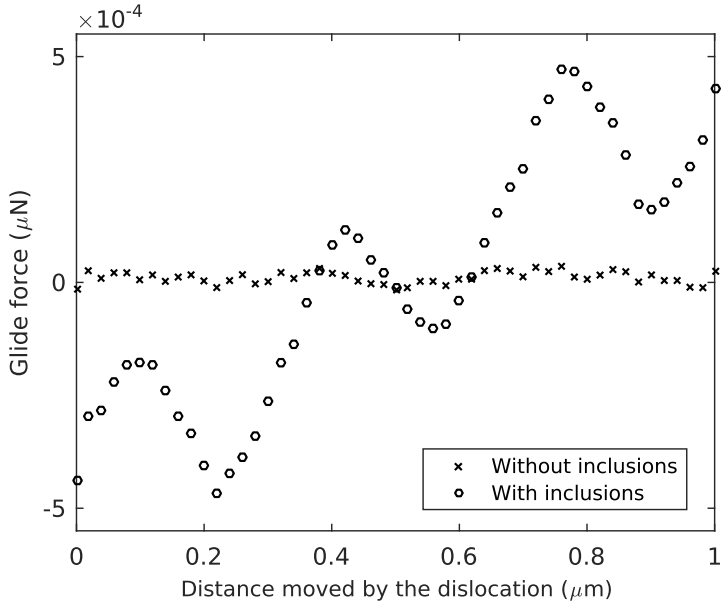

Figure 3.28: The Peach-Koehler force due to elastic mismatch for an edge dislocation near an array of circular inclusions.

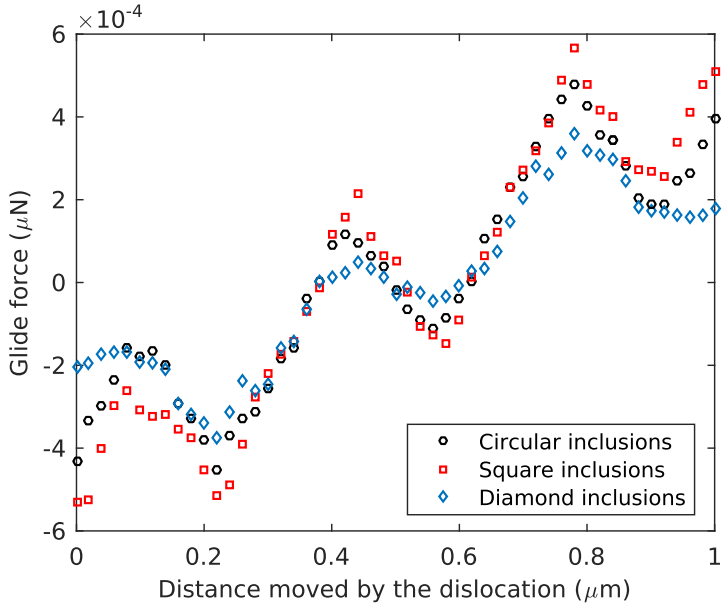

Figure 3.29: A comparison of the Peach-Koehler force due to elastic mismatch for an edge dislocation near an array of circular, square shaped and diamond shaped inclusions.

dislocation moves from one edge of the domain to another as shown in fig. 3.27, it experiences attractive and repulsive forces depending on its location in the domain. The force on the dislocation at the centre of the domain vanishes due to the symmetry in placement of the inclusions. Since the force with which the inclusions attract the dislocation causes the dislocation to move without the need of external influence, the work done on the system (plastic strain created) in moving the dislocation through the domain only involves the force of repulsion acting on the dislocation. Therefore, 1.1×10^{-4} pJ is needed to move the dislocation through a domain containing an array of impenetrable circular inclusions exhibiting elastic mismatch with the corresponding matrix. Correspondingly, a comparison of the Peach-Koehler force due to elastic mismatch for an edge dislocation near an array of circular, square shaped and diamond shaped inclusions in shown in fig. 3.29. Work done in moving the dislocation through a domain filled with square and diamond shaped inclusions is 1.4×10^{-4} pJ and 0.8×10^{-4} pJ respectively. Therefore, more work needs to be done to move a dislocation in a domain with multiple square shaped particles.

When a thermal mismatch between the Al_2Cu precipitates and Al matrix due to a difference in their coefficient of thermal expansion is introduced, the Peach-Koehler force on an edge dislocation is shown in fig. 3.30. On addition of a thermal mismatch to the existing elastic mismatch between the circular inclusions and matrix, 9.1×10^{-3} pJ (an additional 9×10^{-3} pJ) is needed to propel the dislocation through the domain.

When the circular inclusions are replaced with an array of square and diamond shaped inclusions of similar area and material properties, a comparison of the glide force on the dislocation is as shown in fig. 3.31. In case of square and diamond shaped inclusions with elastic as well as thermal mismatch with the matrix, 8.8×10^{-3} pJ and 6.3×10^{-3} pJ respectively is needed to push the dislocation through the domain.

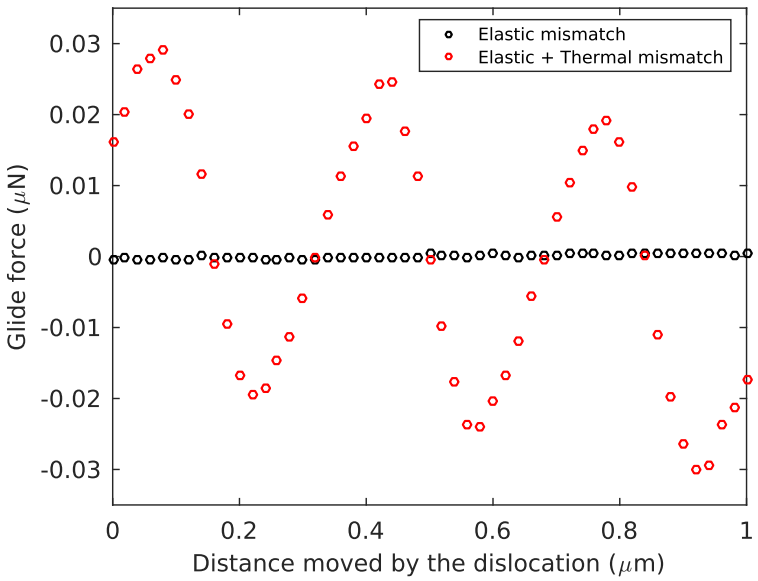

Figure 3.30: The Peach-Koehler force for an edge dislocation near an array of circular inclusions.

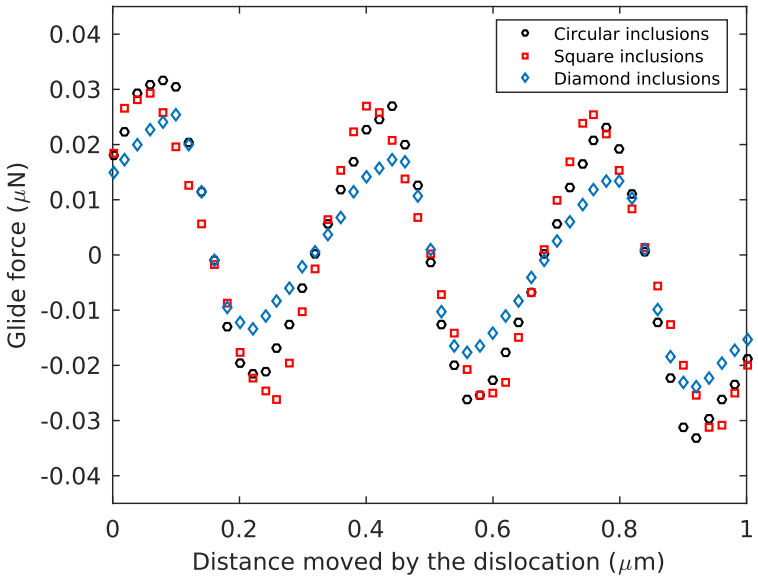

Figure 3.31: A comparison of the Peach-Koehler force due to elastic and thermal mismatch for an edge dislocation near an array of circular, square and diamond shaped inclusions.

Chapter 4

CONCLUSION AND FUTURE WORK

An extended finite element method (XFEM) for modelling the interactions of dislocations with inclusions was presented. A finite element method was used to estimate the stress fields due to configurational forces on the dislocation. The internal discontinuity was introduced across the glide plane in the form of dislocation slip. As the method presented here uses the finite element method to capture stress fields, the mesh needs to be sufficiently refined to capture the singularity at the dislocation core. This method fares better than the standard finite element method in being able to capture the discontinuity in the field variable within a single element. This method eliminates the need to superimpose the image stress fields and analytical infinite domain solutions for determining the Peach-Koehler force, making it computationally more efficient.

The incompatible enrichment scheme based on the Volterra dislocation model involving a sharp cut-off in the discontinuity was considered. The enrichment function was shifted by a certain amount to be able to impose displacement boundary conditions when needed. In addition to the enrichment scheme considered here, other core enrichment functions (compatible core enrichment based on the Peierls-Nabarro model of dislocations) could be developed in accordance with experimental or simulation results and used in lieu of the incompatible enrichment scheme.

Al_2Cu particles in an Al matrix was the system observed in this study. Two orientations of an inclusion in the shape of a square were considered, one with its edges perpendicular to the glide plane was referred to as a square shaped inclusion and the other with its diagonals perpendicular to the glide plane was referred to as a

diamond shaped inclusion.

The outcomes of the study are summarised as follows:

- The proposed method approximates the glide force well and the Peach-Koehler force calculated using the domain form of J-integral converges to the exact solution at an optimal rate for linear finite elements in case of an edge dislocation near a free surface.

- Although the accuracy when using an unstructured mesh reduces slightly in comparison to a structured mesh due to skewed elements, the method converges well.

- A moderate sized contour with an inner radius and outer radius equal to 4 and 8 times the effective element size respectively produces results with only 1% error.

- Integration points as few as 25 along the radial direction and 60 along the angular direction result in as little as 1% error.

- With the above considerations, the domain form of J-integral for a 100×100 element mesh was solved in 3 s on a single CPU PC.

- For an edge dislocation interacting with an impenetrable circular inclusion, the XFEM and exact solutions are in agreement.

- Effect of shape: The force on the dislocation due to elastic mismatch in approaching the centre of a diamond shaped inclusion is 8% more than in approaching the centre of a circular inclusion of equal area.

- Effect of orientation: The force on the dislocation due to elastic mismatch increases by 24% when approaching the centre of a diamond shaped inclusion

instead of a square shaped inclusion.

- Effect of size: When the areas of the inclusions were halved, the dislocation experienced 36% and 30% decrease in force in approaching a square shaped and diamond shaped inclusion, and a circular inclusion respectively.

- On introducing a thermal mismatch between the inclusion and matrix (interface strains equal to 0.004), the force on the dislocation in approaching a circular inclusion grew 15 times.

- In approaching the centre of the top half of the inclusion, the force on the dislocation due to elastic as well as thermal mismatch was 6% and 63% more for a diamond shaped inclusion than a circular or a square shaped inclusion respectively.

- When the dislocation moved towards the top of the inclusion instead, the force on it due to elastic and thermal mismatch was 12% and 56% more for a square shaped inclusion than a circular or a diamond shaped inclusion.

- There was a 34% decrease and 68% increase in the force experienced by the dislocation due to elastic and thermal mismatch in approaching the top of the diamond and square shaped inclusion than in approaching the centre of the top half of the two inclusions respectively. The change in force for a circular inclusion was minuscule.

- The energy needed to push a dislocation through a domain filled with circular inclusions increased 81 times when thermal mismatch was introduced to the elastic mismatch between the inclusions and the matrix.

- The work done to move an edge dislocation through an array of circular inclusions was 4% and 44% more than that needed to move it through an array of square and diamond shaped inclusions respectively.

- In observing the dislocation motion through the domain, the stiffness matrix was assembled only once and the execution time for the assembly and solution of a 100×100 element mesh using Matlab on a single CPU PC was 10 s.

Using the outcomes listed above, the following observations can be made:

- The method proposed here works well for an unstructured mesh. The application of XFEM to an unstructured mesh to study dislocation interactions with inclusions in unprecedented (to the author's knowledge).

- The method is computationally fast and efficient with an error of 1%.

- Sharp corners (centre of a diamond shaped inclusion and top/bottom of a square shaped inclusion) exert a greater force on a dislocation due to stress concentration effects.

- A small spherical inclusion will exert the least force on a dislocation (not considering thermal effects).

- The introduction of eigenstrains increases the force experienced by the dislocation to a large extent.

- A larger amount of work is done in moving a dislocation through a domain filled with circular inclusions.

Increasing the inner radius of the integration domain exceeding what was chosen increased the accuracy slightly but only to a certain point beyond which the accuracy

reduced. Hence, the inner radius must be selected sufficiently far from the dislocation core but yet in the vicinity of the core. Increasing the width of the integration domain was found to increase the accuracy but only to certain value beyond which increasing the domain thickness had next to no effect on the accuracy in calculating the Peach-Koehler force. Doubling the number of integration points along each direction increased the computational time to 8 s and quadrupling it increased the time to 28 s. Since increasing the number of integration points was found to increase the accuracy of the solution up to a certain extent and the amount of computational time needed increased rapidly, a suitable trade-off between the two is necessary for a computationally efficient method.

While none of the existing methods have the adaptability of the proposed method, it does have a few drawbacks of its own that could be addressed in the studies to follow. This study only considered a symmetric array of inclusions, in nature, particle arrays are usually much more disoriented. A dislocation interacting with pristine inclusions was considered in this study, whereas in deformation experiments, dislocations will most likely interact with inclusions as well as debris left behind by previous dislocations in a mechanism examined by Xiang *et al.* (2004). This mechanism used the FFT approach to solve elasticity equations in determining the total stress field of the dislocation, limiting its application to isotropic materials. The proposed method could be used to overcome this handicap and facilitate the calculation of required repulsive forces in anisotropic materials. The inclusions considered here are hard (impenetrable) particles, but they may also occur as misfitting (penetrable) particles and impenetrable misfitting particles. When observing the dislocation-inclusion or dislocation-dislocation interactions (with differently oriented burgers vectors), this method requires more mesh resolution than methods based on superposition and image fields, but its compatibility with standard finite elements ought to make this

method appealing. The method here has been limited to an edge dislocation in 2D, however, its extension to other types of dislocations is straightforward.

REFERENCES

Ames, I., F. d'Heurle and R. Horstmann, "Reduction of electromigration in aluminum films by copper doping", IBM Journal of Research and Development **14**, 4, 461–463 (1970).

Areias, P. and T. Belytschko, "A comment on the article "A finite element method for simulation of strong and weak discontinuities in solid mechanics" by A. Hansbo and P. Hansbo [Comput. Methods Appl. Mech. Engrg. 193 (2004) 3523-3540]", Computer Methods in Applied Mechanics and Engineering **195**, 1275–1276 (2006).

Arsenault, R. and R. Fisher, "Microstructure of fiber and particulate sic in 6061 al composites", Scripta Metallurgica **17**, 1, 67–71 (1983).

Arsenault, R. and N. Shi, "Dislocation generation due to differences between the coefficients of thermal expansion", Materials Science and Engineering **81**, 175–187 (1986).

Batra, R., "The force on a lattice defect in an elastic body", Journal of elasticity **17**, 1, 3–8 (1987).

Beissel, S., G. Johnson and C. Popelar, "An element-failure algorithm for dynamic crack propagation in general directions", Engineering Fracture Mechanics **61**, 3, 407–425 (1998).

Belytschko, T. and T. Black, "Elastic crack growth in finite elements with minimal remeshing", International journal for numerical methods in engineering **45**, 5, 601–620 (1999).

Belytschko, T., J. Fish and B. E. Engelmann, "A finite element with embedded localization zones", Computer methods in applied mechanics and engineering **70**, 1, 59–89 (1988).

Belytschko, T. and M. Fleming, "Smoothing, enrichment and contact in the element-free galerkin method", Computers & Structures **71**, 2, 173–195 (1999).

Belytschko, T. and R. Gracie, "On xfem applications to dislocations and interfaces", International Journal of Plasticity **23**, 10, 1721–1738 (2007).

Belytschko, T., Y. Krongauz, D. Organ, M. Fleming and P. Krysl, "Meshless methods: an overview and recent developments", Computer methods in applied mechanics and engineering **139**, 1, 3–47 (1996).

Belytschko, T., Y. Y. Lu and L. Gu, "Element-free galerkin methods", International journal for numerical methods in engineering **37**, 2, 229–256 (1994).

Belytschko, T., N. Moës, S. Usui and C. Parimi, "Arbitrary discontinuities in finite elements", International Journal for Numerical Methods in Engineering **50**, 4, 993–1013 (2001).

Boniszewski, T. and R. Baker, "Dislocations in manganese sulphide inclusions in steel", Acta Metallurgica **11**, 8, 990–992 (1963).

Bulatov, V. and W. Cai, *Computer simulations of dislocations*, vol. 3 (Oxford University Press on Demand, 2006).

Chawla, K. and M. Metzger, "Initial dislocation distributions in tungsten fibre-copper composites", Journal of Materials Science **7**, 1, 34–39 (1972).

Chessa, J., H. Wang and T. Belytschko, "On the construction of blending elements for local partition of unity enriched finite elements", International Journal for Numerical Methods in Engineering **57**, 7, 1015–1038 (2003).

Devincre, B., L. Kubin, C. Lemarchand and R. Madec, "Mesoscopic simulations of plastic deformation", Materials Science and Engineering: A **309**, 211–219 (2001).

Dolbow, J. and T. Belytschko, "A finite element method for crack growth without remeshing", Int. J. Numer. Meth. Eng **46**, 1, 131–150 (1999).

Dolbow, J., N. Moës and T. Belytschko, "Discontinuous enrichment in finite elements with a partition of unity method", Finite elements in analysis and design **36**, 3, 235–260 (2000).

Duflot, M., "A study of the representation of cracks with level sets", International Journal for Numerical Methods in Engineering **70**, 11, 1261–1302 (2007).

Dundurs, J. and T. Mura, "Interaction between an edge dislocation and a circular inclusion", Journal of the Mechanics and Physics of Solids **12**, 3, 177–189 (1964).

Dundurs, J. and G. Sendeckyj, "Edge dislocation inside a circular inclusion", Journal of the Mechanics and Physics of Solids **13**, 3, 141–147 (1965).

Eshelby, J., "The force on a disclination in a liquid crystal", Philosophical Magazine A **42**, 3, 359–367 (1980).

Eshelby, J. D., "The force on an elastic singularity", Philosophical Transactions of the Royal Society of London A: Mathematical, Physical and Engineering Sciences **244**, 877, 87–112 (1951).

Fleischer, R., "Effects of non-uniformities on the hardening of crystals", Acta Metallurgica **8**, 9, 598–604 (1960).

Fries, T.-P., "A corrected xfem approximation without problems in blending elements", International Journal for Numerical Methods in Engineering **75**, 5, 503–532, URL `http://dx.doi.org/10.1002/nme.2259` (2008).

Fukuzaki, K. and S. Shioya, "On the interaction between an edge dislocation and two circular inclusions in an infinite medium", International journal of engineering science **24**, 12, 1771–1787 (1986).

Fukuzaki, K. and S. Shioya, "On the interaction between an edge dislocation and two circular inclusions in an infinite medium (continued report)", International journal of engineering science **25**, 8, 1017–1027 (1987).

Gardner, D. S. and P. A. Flinn, "Mechanical stress as a function of temperature for aluminum alloy films", Journal of Applied Physics **67**, 4, 1831–1844 (1990).

Gifford, L. N. and P. D. Hilton, "Stress intensity factors by enriched finite elements", Engineering Fracture Mechanics **10**, 3, 485–496 (1978).

Hansbo, A. and P. Hansbo, "A finite element method for the simulation of strong and weak discontinuities in solid mechanics", Computer Methods in Applied Mechanics and Engineering **193**, 3335, 3523 – 3540, URL `http://www.sciencedirect.com/science/article/pii/S0045782504000507` (2004).

Head, A., "Edge dislocations in inhomogeneous media", Proceedings of the Physical Society. Section B **66**, 9, 793 (1953a).

Head, A., "X. the interaction of dislocations and boundaries", The London, Edinburgh, and Dublin Philosophical Magazine and Journal of Science **44**, 348, 92–94 (1953b).

Jirásek, M., "Comparative study on finite elements with embedded discontinuities", Computer Methods in Applied Mechanics and Engineering **188**, 1, 307–330 (2000).

Kim, D.-J., C. A. Duarte and J. P. Pereira, "Analysis of interacting cracks using the generalized finite element method with global-local enrichment functions", Journal of Applied Mechanics **75**, 5, 051107 (2008).

Melenk, J. M. and I. Babuška, "The partition of unity finite element method: basic theory and applications", Computer methods in applied mechanics and engineering **139**, 1, 289–314 (1996).

Moran, B. and C. Shih, "A general treatment of crack tip contour integrals", International Journal of fracture **35**, 4, 295–310 (1987).

Nayroles, B., G. Touzot and P. Villon, "Generalizing the finite element method: diffuse approximation and diffuse elements", Computational mechanics **10**, 5, 307–318 (1992).

Nguyen, V. P., T. Rabczuk, S. Bordas and M. Duflot, "Meshless methods: a review and computer implementation aspects", Mathematics and computers in simulation **79**, 3, 763–813 (2008).

Nicholson, R., G. Thomas and J. Nutting, "The interaction of dislocations and precipitates", Acta Metallurgica **8**, 3, 172–176 (1960).

Noor, A. K., "Global-local methodologies and their application to nonlinear analysis", Finite Elements in Analysis and Design **2**, 4, 333–346 (1986).

Oliver, J., "Modelling strong discontinuities in solid mechanics via strain softening constitutive equations. part 1: Fundamentals", International journal for numerical methods in engineering **39**, 21, 3575–3600 (1996a).

Oliver, J., "Modelling strong discontinuities in solid mechanics via strain softening constitutive equations. part 2: Numerical simulation", International journal for numerical methods in engineering **39**, 21, 3601–3623 (1996b).

Osher, S. and J. A. Sethian, "Fronts propagating with curvature-dependent speed: algorithms based on hamilton-jacobi formulations", Journal of computational physics **79**, 1, 12–49 (1988).

Oswald, J., E. Wintersberger, G. Bauer and T. Belytschko, "A higher-order extended finite element method for dislocation energetics in strained layers and epitaxial islands", International Journal for Numerical Methods in Engineering **85**, 7, 920–938, URL `http://dx.doi.org/10.1002/nme.3011` (2011).

Peach, M. and J. S. Koehler, "The forces exerted on dislocations and the stress fields produced by them", Phys. Rev. **80**, 436–439, URL `http://link.aps.org/doi/10.1103/PhysRev.80.436` (1950).

Rice, J. R., "A path independent integral and the approximate analysis of strain concentration by notches and cracks", Journal of applied mechanics **35**, 2, 379–386 (1968).

Sendeckyj, G., "Screw dislocations in inhomogeneous solids", (1970).

Song, J.-H., H. Wang and T. Belytschko, "A comparative study on finite element methods for dynamic fracture", Computational Mechanics **42**, 2, 239–250 (2008).

Stolarska, M., D. Chopp, N. Moës and T. Belytschko, "Modelling crack growth by level sets in the extended finite element method", International journal for numerical methods in Engineering **51**, 8, 943–960 (2001).

Sukumar, N. and T. Belytschko, "Arbitrary branched and intersecting cracks with the extended finite element method", Int. J. Numer. Meth. Eng **48**, 1741–1760 (2000).

Sukumar, N., D. L. Chopp, N. Moës and T. Belytschko, "Modeling holes and inclusions by level sets in the extended finite-element method", Computer methods in applied mechanics and engineering **190**, 46, 6183–6200 (2001).

Sukumar, N., N. Moës, B. Moran and T. Belytschko, "Extended finite element method for three-dimensional crack modelling", International Journal for Numerical Methods in Engineering **48**, 11, 1549–1570 (2000).

Swenson, D. and A. Ingraffea, "Modeling mixed-mode dynamic crack propagation nsing finite elements: theory and applications", Computational Mechanics **3**, 6, 381–397 (1988).

Taylor, G. I., "The mechanism of plastic deformation of crystals. part i. theoretical", Proceedings of the Royal Society of London. Series A, Containing Papers of a Mathematical and Physical Character **145**, 855, 362–387, URL `http://www.jstor.org/stable/2935509` (1934).

Van der Giessen, E. and A. Needleman, "Discrete dislocation plasticity: a simple planar model", Modelling and Simulation in Materials Science and Engineering **3**, 5, 689 (1995).

Ventura, G., B. Moran and T. Belytschko, "Dislocations by partition of unity", International Journal for Numerical Methods in Engineering **62**, 11, 1463–1487 (2005).

Xiang, Y., D. J. Srolovitz, L.-T. Cheng and E. Weinan, "Level set simulations of dislocation-particle bypass mechanisms", Acta materialia **52**, 7, 1745–1760 (2004).

Zienkiewicz, O. C., R. L. Taylor, O. C. Zienkiewicz and R. L. Taylor, *The finite element method*, vol. 3 (McGraw-hill London, 1977).